

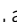



ARTICLE

Leep1 interacts with PIP₃ and the Scar/WAVE complex to regulate cell migration and macropinocytosis

Yihong Yang^{1*}, Dong Li^{1,3*}, Xiaoting Chao^{1,2}, Shashi P. Singh^{4,5} , Peter Thomason^{4,5} , Yonghong Yan⁶, Mengqiu Dong⁶, Lei Li⁷, Robert H. Insall^{4,5} , and Huaqing Cai^{1,2} 

Polarity is essential for diverse functions in many cell types. Establishing polarity requires targeting a network of specific signaling and cytoskeleton molecules to different subregions of the cell, yet the full complement of polarity regulators and how their activities are integrated over space and time to form morphologically and functionally distinct domains remain to be uncovered. Here, by using the model system *Dictyostelium* and exploiting the characteristic chemoattractant-stimulated translocation of polarly distributed molecules, we developed a proteomic screening approach, through which we identified a leucine-rich repeat domain-containing protein we named Leep1 as a novel polarity regulator. We combined imaging, biochemical, and phenotypic analyses to demonstrate that Leep1 localizes selectively at the leading edge of cells by binding to PIP₃, where it modulates pseudopod and macropinocytic cup dynamics by negatively regulating the Scar/WAVE complex. The spatiotemporal coordination of PIP₃ signaling, Leep1, and the Scar/WAVE complex provides a cellular mechanism for organizing protrusive structures at the leading edge.

Introduction

Cell polarity refers to the asymmetry observed in cell shape, structure, or localization of molecular components. Polarity can be organized spontaneously or under the guidance of extracellular biochemical and mechanical cues (Campanale et al., 2017; Goehring and Grill, 2013). Almost all types of cells exhibit some form of polarity, which enables them to carry out diverse functions. For example, in budding yeast, polarity is used for directional growth and division, whereas epithelial cells display both apical–basal and planar polarity, and neurons are polarized with segregated domains of axons and dendrites specialized for receiving and transmitting signals, respectively (Bentley and Banker, 2016; Chiou et al., 2017; Rodriguez-Boulan and Macara, 2014). Considering the range of cellular processes that involve polarity, it is not surprising that misregulation of polarity is associated with developmental disorders and disease (Campanale et al., 2017; Martin-Belmonte and Perez-Moreno, 2012).

Studying cell migration in model systems, such as *Dictyostelium discoideum* and neutrophils, has provided important insights

into the mechanisms underlying the establishment and maintenance of polarity (Artemenko et al., 2014; Devreotes et al., 2017; Graziano and Weiner, 2014; Michael and Vermeren, 2019; Stuelten et al., 2018). In both *Dictyostelium* cells and neutrophils, directed cell migration is initiated when extracellular chemoattractants bind to receptors on the cell surface. Although the chemoattractant receptors are uniformly localized along the plasma membrane (Servant et al., 1999; Xiao et al., 1997), many downstream signaling and cytoskeleton components are localized or activated specifically at either the leading or trailing edge of cells, creating functionally distinct opposing ends that promote cell migration. Events that occur at the leading edge include the activation of several Ras and Rac family GTPases, activation of mTORC2 and its substrates of the Akt/protein kinase B (PKB) family kinases, accumulation of the class I PI3 kinases (PI3Ks) and their product PIP₃, and recruitment of a number of cytoskeletal regulators, such as the Scar/WASP-family verprolin-homologous protein (WAVE) and

¹National Laboratory of Biomacromolecules, Chinese Academy of Sciences Center for Excellence in Biomacromolecules, Institute of Biophysics, Chinese Academy of Sciences, Beijing, China; ²College of Life Sciences, University of Chinese Academy of Sciences, Beijing, China; ³School of Life Sciences, University of Science and Technology of China, Hefei, China; ⁴Cancer Research UK Beatson Institute, Glasgow, UK; ⁵University of Glasgow Institute of Cancer Sciences, Glasgow, UK; ⁶National Institute of Biological Sciences, Beijing, China; ⁷State Key Laboratory of Protein and Plant Gene Research, Peking-Tsinghua Center for Life Sciences, School of Life Sciences, Peking University, Beijing, China.

*Y. Yang and D. Li contributed equally to this paper; Correspondence to Huaqing Cai: huaqingcai@ibp.ac.cn.

© 2021 Yang et al. This article is distributed under the terms of an Attribution–Noncommercial–Share Alike–No Mirror Sites license for the first six months after the publication date (see <http://www.rupress.org/terms/>). After six months it is available under a Creative Commons License (Attribution–Noncommercial–Share Alike 4.0 International license, as described at <https://creativecommons.org/licenses/by-nc-sa/4.0/>).

Arp2/3 complexes responsible for actin polymerization and pseudopod projection (Cai et al., 2010; Charest et al., 2010; Funamoto et al., 2002; Kamimura et al., 2008; Sasaki et al., 2004; Veltman et al., 2014; Veltman et al., 2016). Events that occur at the trailing edge include the recruitment of lipid phosphatase Pten and the generation of formin and myosin II-dependent actin cortex necessary for back retraction (Iijima and Devreotes, 2002; Litschko et al., 2019; Moores et al., 1996; Ramalingam et al., 2015).

Polarized distribution or activation of key signaling and cytoskeleton molecules at the plasma membrane and cortex has implications beyond cell migration. For example, during bulk endocytosis (a general term including macropinocytosis and phagocytosis), many of the leading edge molecules, such as PIP₃, activated Ras or Rac, and the Scar/WAVE and Arp2/3 complexes, localize at the macropinocytic and phagocytic cups (Buckley et al., 2020; Veltman et al., 2016), whereas the trailing edge molecules, such as phosphatase and tensin homolog deleted on chromosome 10 (PTEN), are excluded from the cup areas but occupy the rest of the cell membrane (Hoeller et al., 2013). In addition, during cell division, the leading edge molecules are localized to the poles, whereas the trailing edge molecules are restricted to the cleavage furrow (Janetopoulos and Devreotes, 2006; King et al., 2010). Furthermore, these asymmetrically localized molecules exhibit signature behaviors in cells stimulated with chemoattractants. For example, upon the addition of uniform cAMP, many of the leading edge molecules translocate transiently to the cell periphery within ~10 s and redistribute to the cytosol by 30 s. With the same kinetics, the trailing edge molecules transiently fall off from the cell periphery and into the cytosol before returning to the cell membrane or cortex (Sobczyk et al., 2014; Swaney et al., 2010).

Establishing morphologically and functionally distinct subregions is important for cell polarity, but many aspects of this complex process are not fully understood, such as how signaling and cytoskeleton regulators are selectively targeted during different morphological states and how their activities are integrated over space and time to enable diverse cell functions. Taking advantage of the observation that both leading and trailing edge molecules respond to chemoattractant stimulation by transiently relocalizing with respect to the cell periphery, we developed a proteomics approach to comprehensively identify polarity regulators by isolating proteins exhibiting signature spatiotemporal changes following stimulation. Using this approach, we identified a leucine-rich repeat (LRR) domain-containing protein we named leading edge enriched protein 1 (Leep1) as a novel leading edge-localized polarity regulator, which interacts with PIP₃ and the Scar/WAVE complex to modulate protrusion dynamics.

Results

Proteomics-based approach to identify polarity regulators

As many signaling molecules involved in polarity regulation exhibit characteristic translocation behaviors upon chemoattractant stimulation, we designed a proteomics-based approach to identify novel polarity regulators (Fig. 1 A). Cells were differentiated to induce chemotactic sensitivity, stimulated with 1 μM cAMP,

and rapidly lysed at 0, 10, 20, and 60 s. For each time point, membrane fractions were collected and treated with sodium carbonate to extract peripherally associated proteins. The peripheral membrane protein fractions were then concentrated by TCA precipitation and fractionated by SDS-PAGE followed by tryptic in-gel digestion, peptide extraction, and mass spectrometry (MS) analysis. Based on the translocation property of known regulators, we expected leading edge proteins to be enriched, and lagging edge proteins depleted, in samples collected at the middle two time points.

We validated our approach using PHcrac, the Pleckstrin homology (PH) domain from the cytosolic regulator of adenylate cyclase (CRAC), which was discovered in *Dictyostelium* as a PI(3,4)P₂/PIP₃ binding protein involved in chemotactic signaling (Huang et al., 2003; Parent et al., 1998). As reported previously, following cAMP stimulation, PHcrac-GFP translocated briefly from the cytosol to the plasma membrane and then returned to the cytosol (Fig. 1 B). Consistently, it was enriched in the membrane, peripheral membrane, and TCA precipitated membrane fractions collected at 10 and 20 s (Fig. 1 C). Furthermore, the dynamics recorded in the MS analysis closely matched the results from Western blotting. The protein scores at 0, 10, 20, and 60 s, which likely included contributions from the endogenous CRAC protein, were 3.21, 76.03, 60.62, and 17.12, respectively (Table S1, Table S2, and Table S3). These results indicate that the method we developed is able to capture the transient translocation response exhibited by polarity proteins such as PHcrac.

Following the MS analysis, we obtained a dataset of 2,069 proteins after filtering out those with less than three peptides in the samples from 10 or 20 s to ensure the reliability of the profile (Table S1, Table S2, and Table S3). We defined a translocation score (the sum of protein scores at 10 and 20 s divided by the sum of all four time points) for each protein (Fig. 1 D). Putative polarity regulators that responded to stimulation by translocating to or falling off from the plasma membrane would exhibit high or low translocation scores, respectively, whereas proteins that underwent no localization changes would show scores approaching 0.5. We found that ~70% of proteins (1,439 out of 2,069) had negligible changes in abundance in the peripheral membrane protein pool and, therefore, had scores within the range of 0.45 to 0.55 (Table S1, Table S2, and Table S3).

Proteins with scores significantly deviating from the average were categorized further. Among the proteins with scores ≥0.55, we obtained 164 proteins that shared translocation profiles as PHcrac (Table S2). Remarkably, these proteins include a series of well-characterized signaling or cytoskeletal proteins that participate in leading edge activities, such as ForG, PkbA, PhdA, RGBARG, MyoB, and myosin IE (Fig. 1 E and Table S3; Brzeska et al., 2016; Buckley et al., 2020; Chen et al., 2012; Dürrwang et al., 2006; Funamoto et al., 2001; Junemann et al., 2016; Meili et al., 1999). In contrast, proteins including myosin II and corticellins (Clow and McNally, 1999; Ramalingam et al., 2015), which are lagging edge regulators known to have an opposite pattern of translocation, showed lower scores (<0.45; Table S3). These experiments validated the approach as a convenient

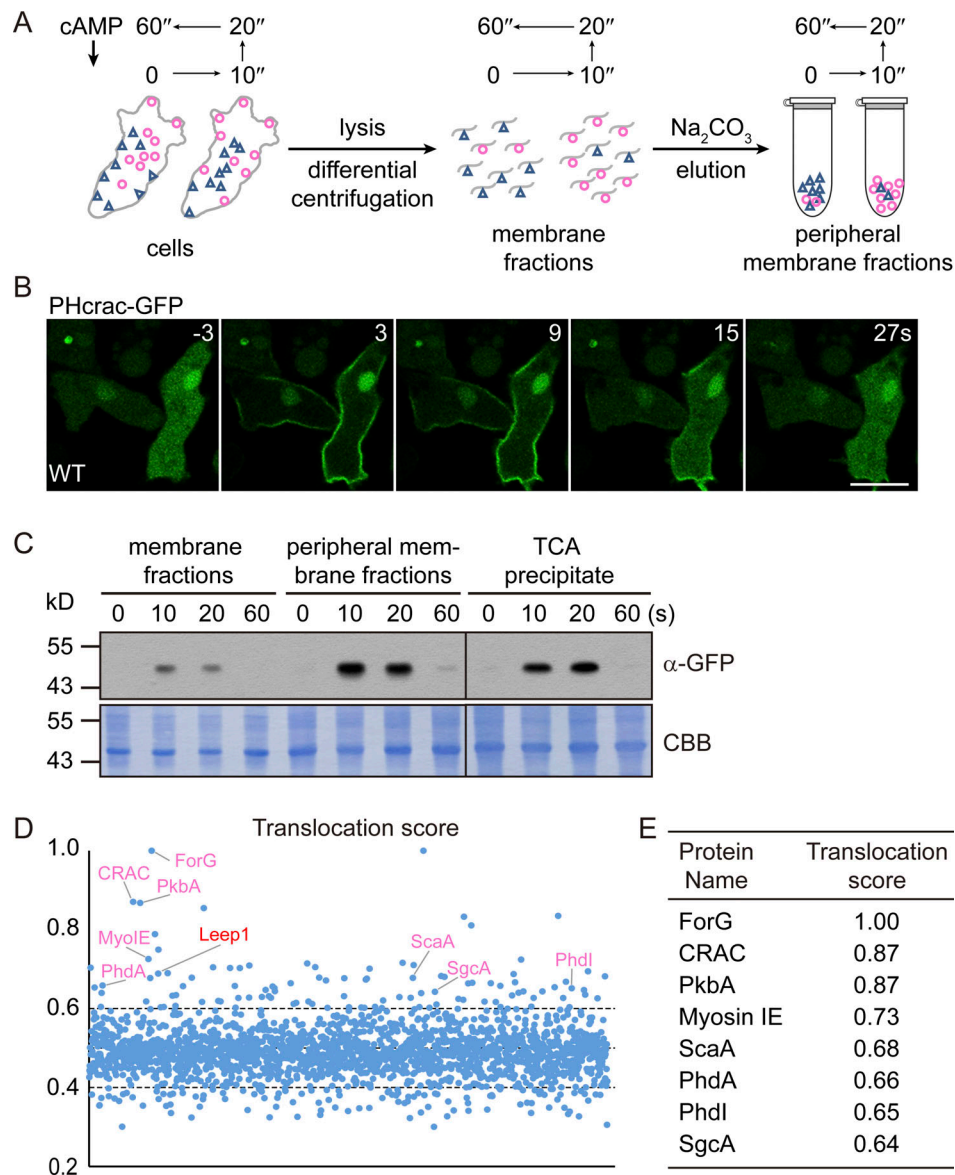


Figure 1. Proteomic analysis of cAMP-induced translocation. (A) Outline of the proteomic experiment for identification of polarity regulators. Red circles and blue triangles symbolize potential leading and lagging edge proteins, which transiently translocate to or dissociate from the plasma membrane upon stimulation, respectively, and hence accumulate differentially in the peripheral membrane protein fractions. (B) PHcrac-GFP translocation upon the addition of cAMP at time 0. Scale bar = 10 μ m. (C) Cells expressing PHcrac-GFP were stimulated with cAMP, lysed at the indicated time points, and processed to obtain different membrane fractions, which were then probed with an anti-GFP antibody. PHcrac-GFP was found to be enriched in fractions collected at 10 and 20 s. CBB, Coomassie Brilliant Blue. (D and E) Plot of the translocation scores of 2,069 proteins identified in the MS analysis, with each dot representing a protein. Several known leading edge regulators are marked on the graph, and their respective translocation scores are listed in E. The translocation score of Leep1 is 0.69.

strategy for systematic isolation of proteins with asymmetric distribution. Of the uncharacterized proteins exhibiting dynamic patterns as PHcrac, this report focuses on the characterization of Leep1 (translocation score, 0.69; gene ID, DDB_G0293920).

Leep1 is a leading edge protein

We first examined whether Leep1 responds to chemoattractant stimulation. We expressed GFP-Leep1 in WT cells, allowed the cells to differentiate, and then stimulated them with cAMP. Consistent with the MS data, GFP-Leep1 transiently redistributed

to the cell periphery after stimulation (Fig. 2, A-C; and Video 1). GFP-Leep1 also responded to folic acid, the chemoattractant for undifferentiated vegetative cells (Fig. 3 A). As discussed previously, such redistribution is a hallmark of leading edge proteins. We further characterized the localization of Leep1 in vegetative and differentiated cells.

Vegetative cells of axenic strains produce distinct protrusive structures, particularly macropinocytic and phagocytic cups for bulk endocytosis and pseudopods for cell movement. We found that in cells actively performing macropinocytosis, Leep1 was specifically enriched at membrane patches that invaginated to

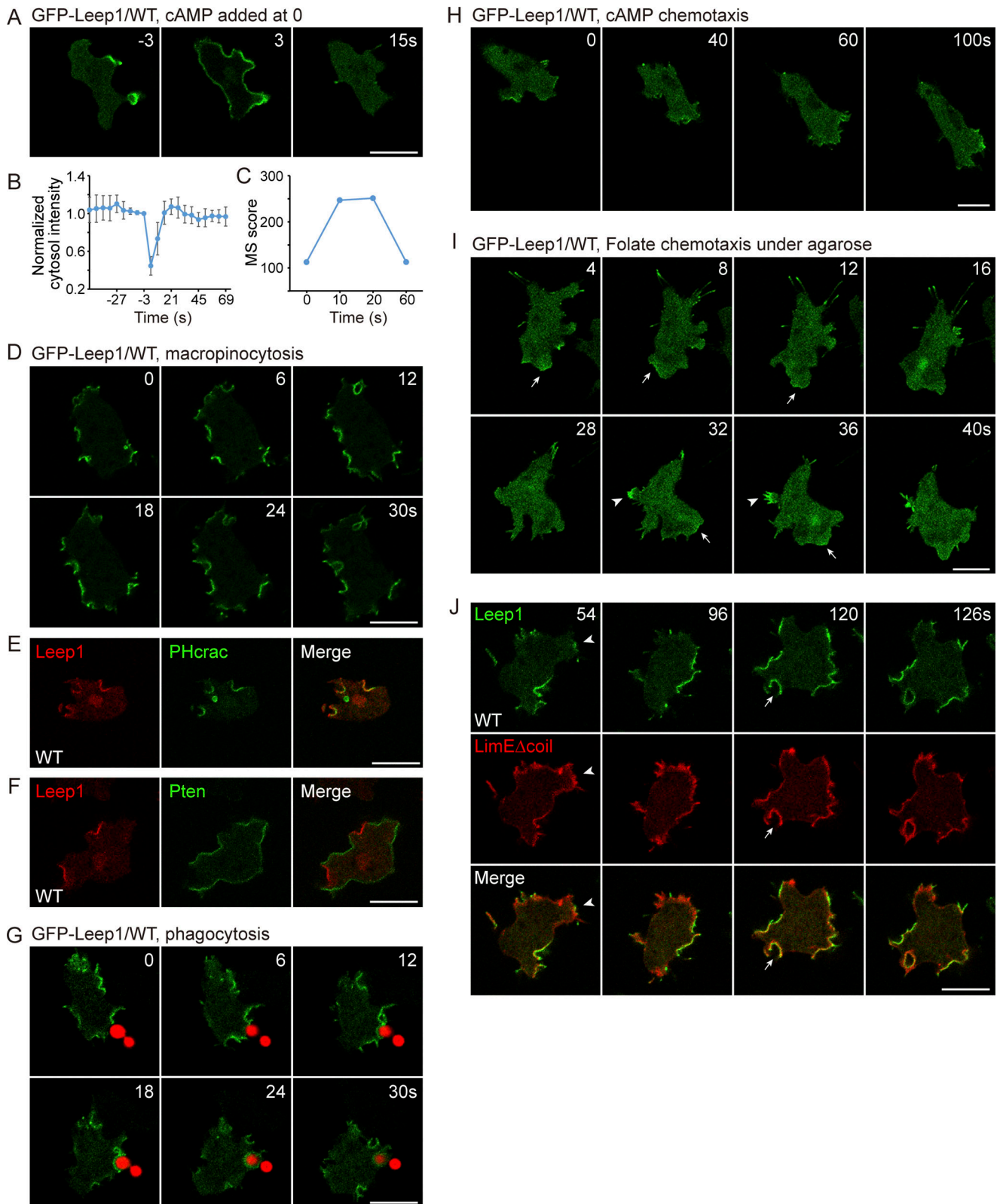


Figure 2. Localization of Leep1 in vegetative and developed cells. (A) GFP-Leep1 translocation in response to cAMP stimulation. **(B)** Quantification of Leep1 translocation (mean \pm SD; $n = 6$ cells from three videos). **(C)** MS scores for Leep1 at the respective time points. **(D)** GFP-Leep1 localization during macropinocytosis. **(E)** RFP-Leep1 colocalizes with PHcrac-GFP at macropinocytic cups. **(F)** RFP-Leep1 and Pten-GFP exhibit complementary distributions on the plasma membrane. **(G)** GFP-Leep1 localization during phagocytosis of TRITC-labeled yeast. **(H)** GFP-Leep1 localization in cells chemotaxing toward cAMP. A micropipette filled with cAMP was placed at the bottom right corner. **(I)** GFP-Leep1 localization in cells moving along a self-generated folate gradient. Arrows point to front protrusions; arrowheads point to retracting pseudopods. **(J)** Time-lapse imaging of cells coexpressing GFP-Leep1 and the F-actin marker LimE Δ coil-RFP. Arrowheads point to pseudopod-type protrusions; arrows point to macropinocytic cups. Scale bars = 10 μ m.

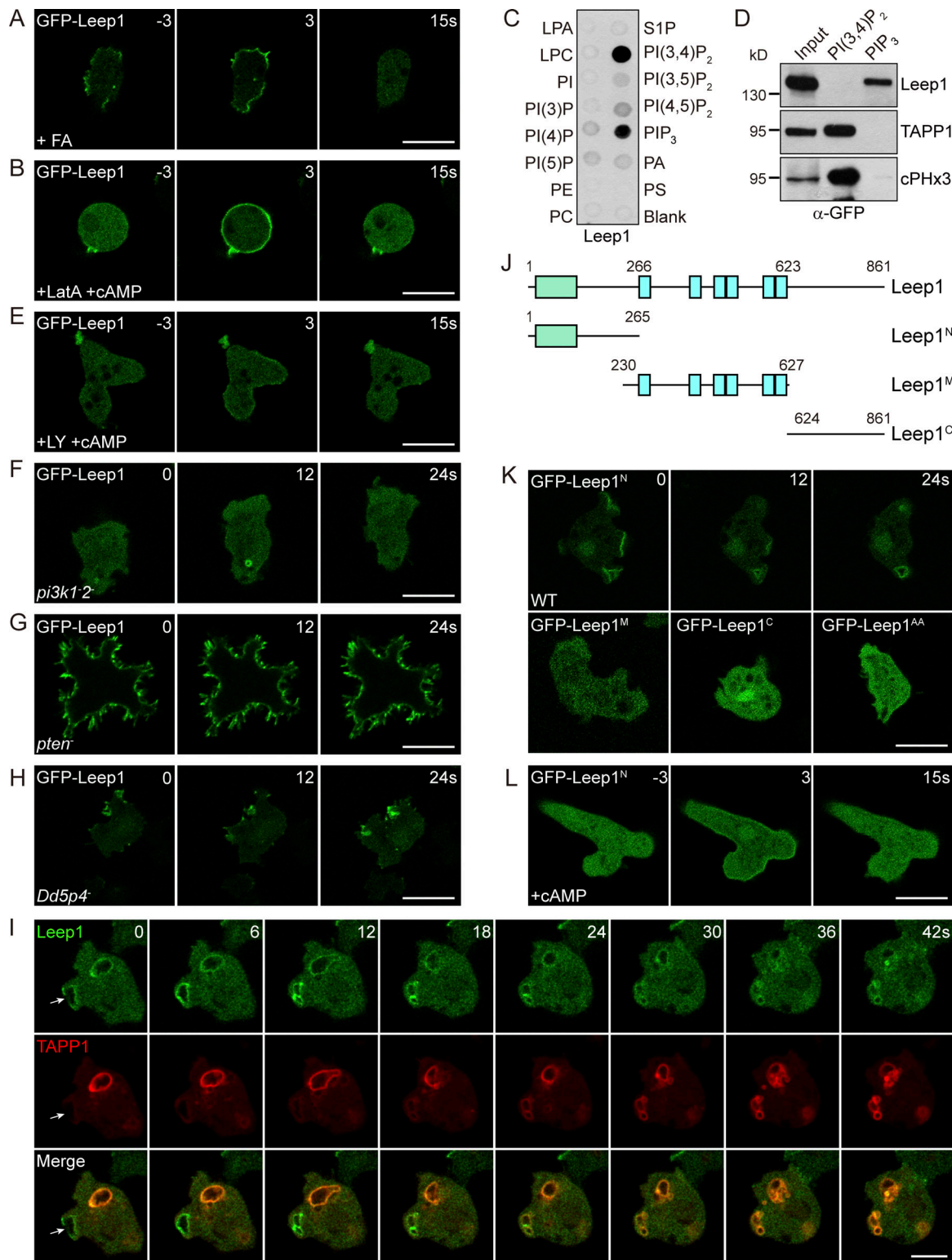


Figure 3. **Leep1 localizes to the leading edge by association with PIP₃.** (A and B) GFP-Leep1 translocation in response to folic acid (FA; A) or cAMP in the presence of LatA (B). (C) Lipid dot blot assay using GFP-Leep1 cell lysates. (D) Cells lysates containing GFP-tagged Leep1, TAPP1, or cPHx3 were incubated with PI(3,4)P₂- or PIP₃-coated agarose beads. Proteins eluted from the beads were probed with anti-GFP antibody. Lysate (2.4%) was loaded as input. (E) GFP-Leep1 translocation in response to cAMP in the presence of LY294002. (F–H) GFP-Leep1 localization in cells lacking the respective phosphoinositide kinases or phosphatases. (I) Sequential accumulation of GFP-Leep1 and TAPP1-RFP. GFP-Leep1 was enriched at membrane ruffles and macropinosytic cups and quickly removed from internalized macropinosomes, whereas the signal of TAPP1 gradually increased until a peak was reached after the macropinosomes detached from the cell surface. (J) A schematic representation of full-length Leep1 and truncation constructs. The green bar represents a putative PH domain-like fold (aa 17–115) and cyan bars a series of LRRs. (K) Localization of the N-terminal (Leep1^N), middle (Leep1^M), and C-terminal (Leep1^C) fragments of Leep1, and Leep1 mutated at lysine 28 and arginine 39 (Leep1^{AA}). (L) Leep1^N mediates cAMP-stimulated translocation. Scale bar = 10 μm.

form macropinocytic cups and dispersed shortly after cup closure (Fig. 2 D and Video 1). Consistently, Leep1 largely overlapped with PHcrac at macropinocytic cups (Fig. 2 E). Furthermore, Leep1 was excluded from sites where the PIP₃ phosphatase, Pten, accumulated (Fig. 2 F). Similar spatiotemporal distribution was observed in cells producing phagocytic cups. When taking in yeast particles, Leep1 localized to nascent phagocytic cups, remained associated with the membrane over the course of engulfment, and was shed from phagosomes as they moved into the cells (Fig. 2 G).

In contrast to the strongly enriched signals at macropinocytic cups, Leep1 was more sporadically recruited to pseudopods in randomly moving cells. A similar pattern was seen in differentiated cells chemotaxing toward cAMP (Fig. 2 H and Video 2) or vegetative cells moving along a self-generated folate gradient (Fig. 2 I and Video 3). In the latter case, the folate contained within the agarose was locally degraded by secreted and cell-surface deaminase, creating a steep gradient that moved along with the chemotaxing cells as they traversed long distances (Tweedy et al., 2016; Woznica and Knecht, 2006). The pressure of the agarose also suppressed macropinocytosis (Veltman et al., 2014). Leep1 signals were detected at protrusions at the migrating front as well as those on the lateral side that retracted into the cells (Fig. 2 I).

We coexpressed GFP-Leep1 with LimΔcoil-mRFP, a marker for newly polymerized actin, to further document the distribution of Leep1 in vegetative cells (Fig. 2 J and Video 4). In randomly migrating cells, pseudopods are commonly seen as convex and spiky actin-filled protrusions in the direction of forward cell movement, though sometimes it is difficult to discriminate them from nascent macropinosomes, especially if the latter structures abort without vesicle formation (Veltman et al., 2014; Veltman et al., 2016). As shown in Fig. 2 J, at 54 and 96 s, LimEΔcoil was enriched on the convex pseudopod-type protrusions, where Leep1 was weakly recruited; at 120 and 126 s, when a macropinocytic cup formed, the two proteins extensively colocalized on the negatively curved region. Together these experiments indicate a potential contribution of Leep1 in specialized leading edge activities.

Leep1 localizes to the leading edge by association with specific phospholipids

To determine how Leep1 localizes to the leading edge, we tested whether an intact actin cytoskeleton is required for its redistribution during stimulation. We disrupted the actin cytoskeleton by treating cells with 5 μM Latrunculin A (LatA), which caused the cells to lose polarity and round up (Fig. 3 B). This morphological change initially resulted in the distribution of GFP-Leep1 to the cytosol. However, when stimulated with cAMP, GFP-Leep1 could still translocate to the plasma membrane (Fig. 3 B).

As Leep1 and PHcrac share actin-independent translocation, we examined whether the localization of Leep1 is regulated by phosphoinositide signals like PHcrac. Several lines of evidence indicate that PIP₃ plays a key role. First, when incubated with PIP strips or PIP-coated agarose beads, GFP-Leep1 bound specifically to PIP₃ and PI(3,4)P₂ (Fig. 3, C and D), with a preference

for PIP₃ in the bead pull-down assay (Fig. 3 D). Second, the membrane localization and cAMP-induced translocation of Leep1 were largely abolished by the PI3K inhibitor LY294002 (Fig. 3 E) or deleting the two major PI3Ks in cells (Fig. 3 F and Fig. S1 A; Buczynski et al., 1997; Hoeller et al., 2013), but greatly enhanced in *pten*⁻ cells, which have globally increased PIP₃ (Fig. 3 G; Iijima and Devreotes, 2002). In contrast, deleting Dd5P4, a homologue of the mammalian inositol 5-phosphatase OCRL proposed to produce PI(3,4)P₂ (Loovers et al., 2007), did not affect the asymmetric distribution of Leep1 (Fig. 3 H), though the mutant was impaired in localization of the PI(3,4)P₂ sensor TAPP1 and macropinocytosis, as expected (Fig. S1 B). Third, in response to cAMP stimulation, the PIP₃ binding protein PH_{GRP1} (Dormann et al., 2004; Klarlund et al., 1997) translocated like Leep1 and PHcrac (Fig. S1 C), whereas neither of the PI(3,4)P₂ specific sensors, TAPP1 or cPH×3 (Goulden et al., 2019; Fig. 3 D), exhibited detectable translocation (Fig. S1 C). Finally, Leep1 colocalized with PHcrac at macropinocytic cups but dissociated before PHcrac (Fig. 2 E) or the PI(3,4)P₂ sensors (Fig. 3 I and Fig. S1 D) from internalized macropinosomes. These observations are in line with previous studies suggesting that PIP₃ is converted into PI(3,4)P₂ during macropinocytosis (Maekawa et al., 2014). Together, these experiments indicate that PIP₃ is primarily responsible for recruiting Leep1 to protrusions and during stimulation.

We characterized the domain composition of Leep1 to search for regions responsible for membrane binding. Sequence analysis revealed that the central 358 aa are comprised of a series of structural unit known as LRRs (Fig. 3 J). LRRs adopt a β strand-turn-α helix structure containing 20–30 aa that are rich in leucine; tandem repeats of LRRs generally fold together to form a horseshoe-shaped protein domain, which is thought to provide structural framework for protein–protein interactions (Kobe and Kajava, 2001). We generated GFP-tagged truncation constructs covering the middle LRR region and the N or C fragments (Fig. 3 J). Leep1^N localized to the macropinocytic cups and was able to respond to cAMP stimulation, whereas Leep1^M and Leep1^C localized to the cytoplasm (Fig. 3, K and L). We further investigated the role of Leep1^N. Structural modeling using the protein homology/analogy recognition engine 2 (Phyre2) revealed a PH domain-like fold within this region (aa 17–115) and overall structural similarity to Carmil proteins, which are conserved actin regulators first discovered and named in *Dictyostelium* (Jung et al., 2001). Intriguingly, the solved structure of mouse CARMIL1 also contains a noncanonical PH domain at the N terminus (Zwolak et al., 2013). Sequence alignment of Leep1 with known PIP-binding PH domains from *Dictyostelium* uncovered two conserved positively charged residues, K28 and R39, in the β1/β2 loop (Fig. S1 E). Charged residues within these loops have been shown to be essential for the interactions of PH domains with phospholipids (Lemmon, 2004). When the two residues were mutated to alanines, Leep1^{AA} no longer associated with the plasma membrane (Fig. 3 K). These experiments indicate that the N terminus of Leep1 likely folds as a PH domain, interacting with PIP₃ to mediate the leading edge localization.

Leep1 regulates macropinocytosis and pseudopod dynamics

To analyze the function of Leep1, we generated independent knockout mutants by homologous recombination (Fig. S2, A and B). When initially assessed on bacterial lawns, plaque growth of the knockout cells was indistinguishable from that of WT, indicating that bacterial uptake, subsequent digestion, and multicellular development were not affected (Fig. S2 C). Consistently, when the knockout cells were plated on non-nutrient agar, they differentiated and formed streams of migrating cells and fruiting bodies similar to WT (Fig. S2 D).

The macropinocytic cup localization of Leep1 prompted us to examine the efficiency of fluid phase uptake. The accumulation of 70 kD dextran in cells shortly after addition was demonstrated to reflect the rate of macropinocytosis (Hacker et al., 1997). We found that the two knockout mutants exhibited an ~35% reduction in the rate of macropinocytosis compared with WT in the microscopy experiment after a 30-min incubation with tetramethylrhodamine isothiocyanate (TRITC)-dextran (Fig. 4, A and B). A similar defect was observed with flow cytometry analysis (Fig. 4 C). Consistent with the notion that macropinocytosis is the major route by which axenically grown cells obtain nutrients (King and Kay, 2019), we found that the generation time in liquid medium increased from ~9.5 h for WT to ~15 h for the knockout cells (Fig. 4 D). The two knockout clones exhibited identical phenotypes; therefore, we used one clone in all later experiments, henceforth referred to as *leep1*⁻ cells.

We expressed PHcrac-GFP in WT and *leep1*⁻ cells to visualize macropinocytosis dynamics (Fig. 4 E and Video 5). WT cells constantly formed thin sheet-like protrusions labeled by PHcrac-GFP, which quickly matured into closed vesicles. Despite the production of similar-sized ruffles (Fig. 4 F), the progression to negatively curved cups frequently stalled in *leep1*⁻ cells, causing PHcrac-labeled patches to remain planar for prolonged periods of time, abort without vesicle formation, or proceed with the formation of small vesicles (Fig. 4 E). Quantification revealed that the number of closed macropinocytic cups per cell per minute was reduced by ~30% in *leep1*⁻ cells (Fig. 4 G), confirming the role of Leep1 in promoting macropinocytosis. However, *leep1* deletion did not affect phagocytosis of yeast or bacteria particles (Fig. 4 H; and Fig. S2, E-G). Compared with phagocytosis, macropinocytosis relies more heavily on spontaneous activation of the signaling and cytoskeleton network, which drives cup formation independently of physical template or surface receptor (King and Kay, 2019; Veltman et al., 2016). This may underlie the differential requirement for Leep1 in the two forms of endocytosis.

GFP-Leep1 was also detected at pseudopods (Fig. 2, H-J). To examine whether Leep1 regulates cell migration, we compared the motile behavior of WT and *leep1*⁻ cells in random motility assays. The average speed and directness were only marginally affected by *leep1* deletion (Fig. S2 H). We employed under-agarose assays to quantitatively measure directed cell migration. In the experiments, cells were exposed to either a passive gradient (Fig. S2 I) or a self-generated gradient of folate (Fig. 4 I and Video 6). The *leep1*⁻ cells migrated up the gradient under both conditions with comparable speed, directness, and chemotactic index to WT. However, a more careful assessment of

pseudopod dynamics revealed that *leep1*⁻ cells generated fewer pseudopod splitting events compared with WT (1.2/min versus 2.3/min; Fig. 4 J and Video 7). Tracks of WT cells expressing GFP-ArpC4, a subunit of the Arp2/3 complex, showed continuous runs, which were interspersed with steps where the leading edge split, whereas those of *leep1*⁻ cells expressing GFP-ArpC4 showed a smoother progression (Davidson et al., 2018). Therefore, although Leep1 is dispensable for directed cell migration, it appears to fine-tune pseudopod dynamics. These experiments support a distinctive role of Leep1 in regulating leading activities.

Overexpression of Leep1 alters cytoskeleton rearrangement

In addition to altered macropinocytosis and pseudopod dynamics observed in the *leep1*⁻ cells, another clue regarding the function of Leep1 was provided by overexpression experiments. We noted that, when expressed at high levels, Leep1 altered cell morphology by inducing filopodia formation. As shown in Fig. 5 A, when Leep1 was expressed from extrachromosomal plasmids, cells with various degrees of expression could be observed. The low-expressing cells exhibited a rather normal morphology, with a few filopodia and Leep1 decorating the macropinocytic cups, whereas the high-expressing cells exhibited an increase in the number of substrate-attached and free filopodia and shallow macropinocytic cups. We confirmed that these spiky projections were filopodia by staining cells with Alexa Fluor 555-phalloidin (Fig. 5, A and B) or coexpressing RFP-Leep1 with GFP-myosin VII, which demarks the tips of mature and growing filopodia (Fig. 5 D; Tuxworth et al., 2001).

When different Leep1 truncations or mutations were expressed, it became evident that the filopodia-promoting activity requires an intact C terminus and membrane binding. This activity was not affected by removing up to 125 aa from the C terminus (Leep1¹⁻⁷³⁶) but was partly reduced by further truncation (Leep1¹⁻⁶⁷²) and abolished by deleting the sequences after the LRR region (Leep1¹⁻⁶²³; Fig. 5 B and Video 8). In contrast to Leep1- and Leep1¹⁻⁷³⁶-overexpressing cells, which frequently contained >15 and sometimes up to 40–50 filopodia, Leep1^N- and Leep1¹⁻⁶²³-overexpressing cells usually had 5–10 filopodia. Scanning electron micrographs illustrated similar findings (Fig. 5 C). However, the C terminus of Leep1 was not sufficient to promote filopodia formation. The membrane binding-defective Leep1^{AA} did not cause excessive filopodia when overexpressed (Fig. 5 B).

We suspected that unconstrained filopodia production may be incompatible with other actin-based activities. Compared with GFP-Leep1^N- and GFP-Leep1¹⁻⁶²³-expressing cells, in which prominent macropinocytic cups decorated by the fusion proteins were frequently observed, Leep1-overexpressing cells were more flattened, with smaller and shallower cups (Fig. 5, A and B). To confirm that Leep1 overexpression negatively impacts macropinocytosis, we measured dextran uptake. Cells expressing different GFP-fusion proteins were divided into two categories: the low expressers containing the dimmer 50% of cells, and the high expressers containing the brighter 50%. For Leep1 and Leep1¹⁻⁶⁷², strongly fluorescent cells tended to accumulate less dextran (Fig. 5, E and F), and this effect scaled positively

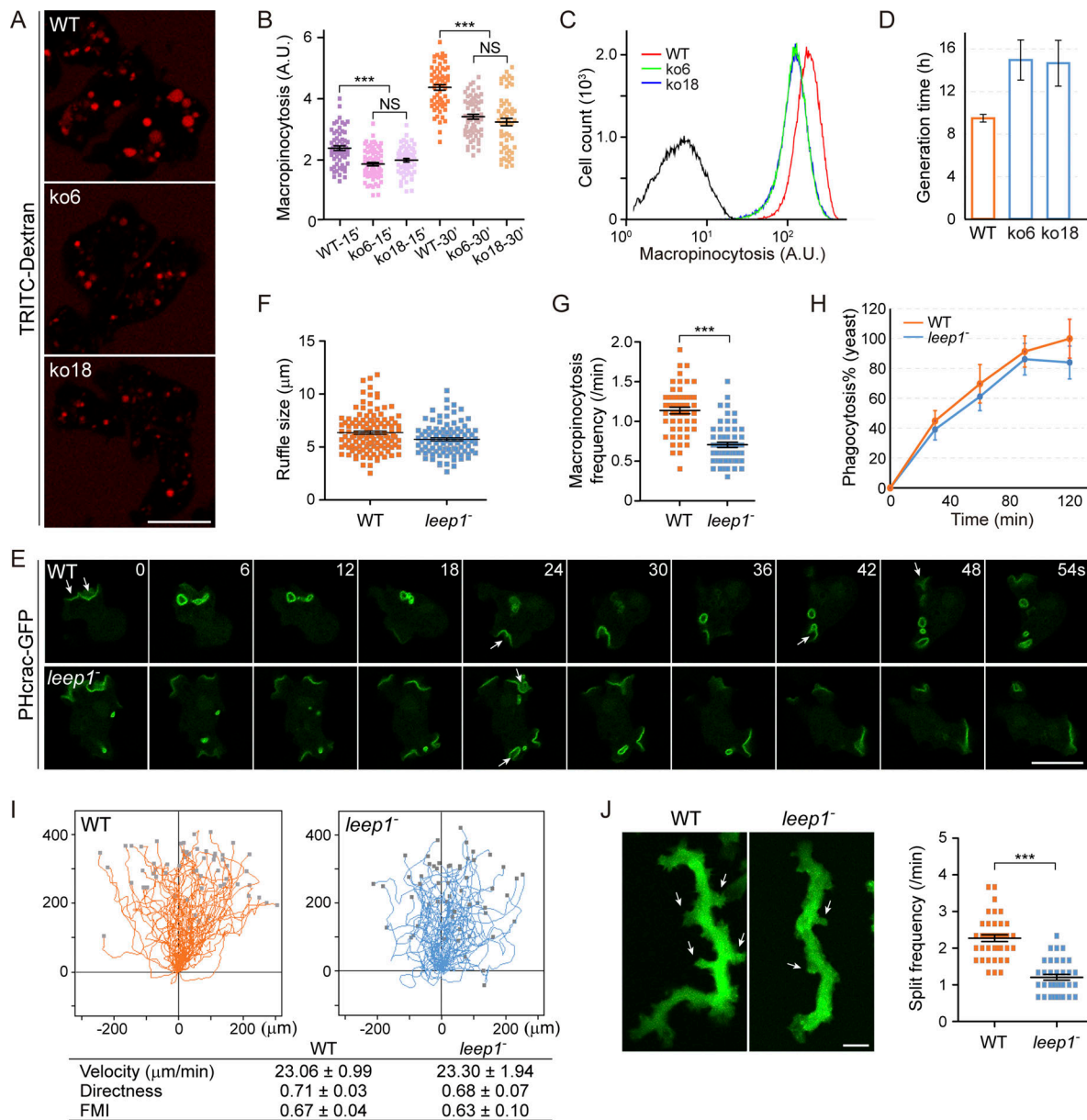


Figure 4. Leep1 regulates macropinocytic cup and pseudopod dynamics. (A) TRITC-dextran uptake in the WT and two independent knockout (ko) clones. Images were acquired after 30 min of incubation. (B) Quantification of dextran uptake ($n = 60, 74, 60, 61, 64,$ and 58 for the samples listed from left to right). (C) Macropinocytosis competence determined by flow cytometry analysis of WT (red), ko6 (green), and ko18 (blue) cells incubated with TRITC-dextran for 30 min or WT cells incubated without TRITC-dextran (black). Each sample represents $\sim 100,000$ cells. (D) Cell growth measured by generation time. (E) Time-lapse imaging of PHcrac-GFP in WT and *leep1⁻* cells. Arrows point to macropinocytic cups that closed. (F) Quantification of ruffle size ($n = 120$ for WT and 97 for *leep1⁻*). (G) Quantification of the frequency of macropinosome formation ($n = 53$ for WT and 58 for *leep1⁻*). (H) Quantification of phagocytosis of TRITC-labeled yeast. (I) Top: Trajectories of cells migrating under agarose against self-generated folate gradients ($n = 60$ for WT and 55 for *leep1⁻*). Bottom: Summary of the respective chemotaxis parameters. (J) Quantification of pseudopod split events in WT and *leep1⁻* expressing GFP-ArpC4 during under-agarose chemotaxis ($n = 39$ for WT and 34 for *leep1⁻*). Images on the left show representative tracks, with each pixel corresponding to the maximum pixel intensity for that location over the course of the video. Data in B, F, G, and J were from at least two independent experiments, and n represents the number of cells or events (for F) quantified. Graphs in C and I are from one representative experiment out of three independent experiments. Data in D, H, and the bottom panels of I were from three independent experiments and represent mean \pm SD. The scatter plots show data points with means and SEM. Significance was determined by one-way ANOVA in B and t test with Welch's correction in F, G, and J (NS, $P > 0.05$; ***, $P < 0.001$). Scale bar = $10 \mu\text{m}$. A.U., arbitrary units; FMI, forward migration index.

with the degree of overexpression (Fig. 5, G and H). In contrast, overexpression of Leep1¹⁻⁶²³ or GFP had no effect (Fig. 5 F). Thus, an actin cytoskeleton remodeling capability is associated with Leep1, which likely underlies the need to fine-tune its level for optimal leading edge function.

Leep1 interacts with the Scar/WAVE complex to regulate leading edge activities

How might Leep1 link membrane binding with cytoskeleton remodeling to regulate leading edge activities? Leep1 shares sequence similarity with CARMIL proteins (26.7% identity and

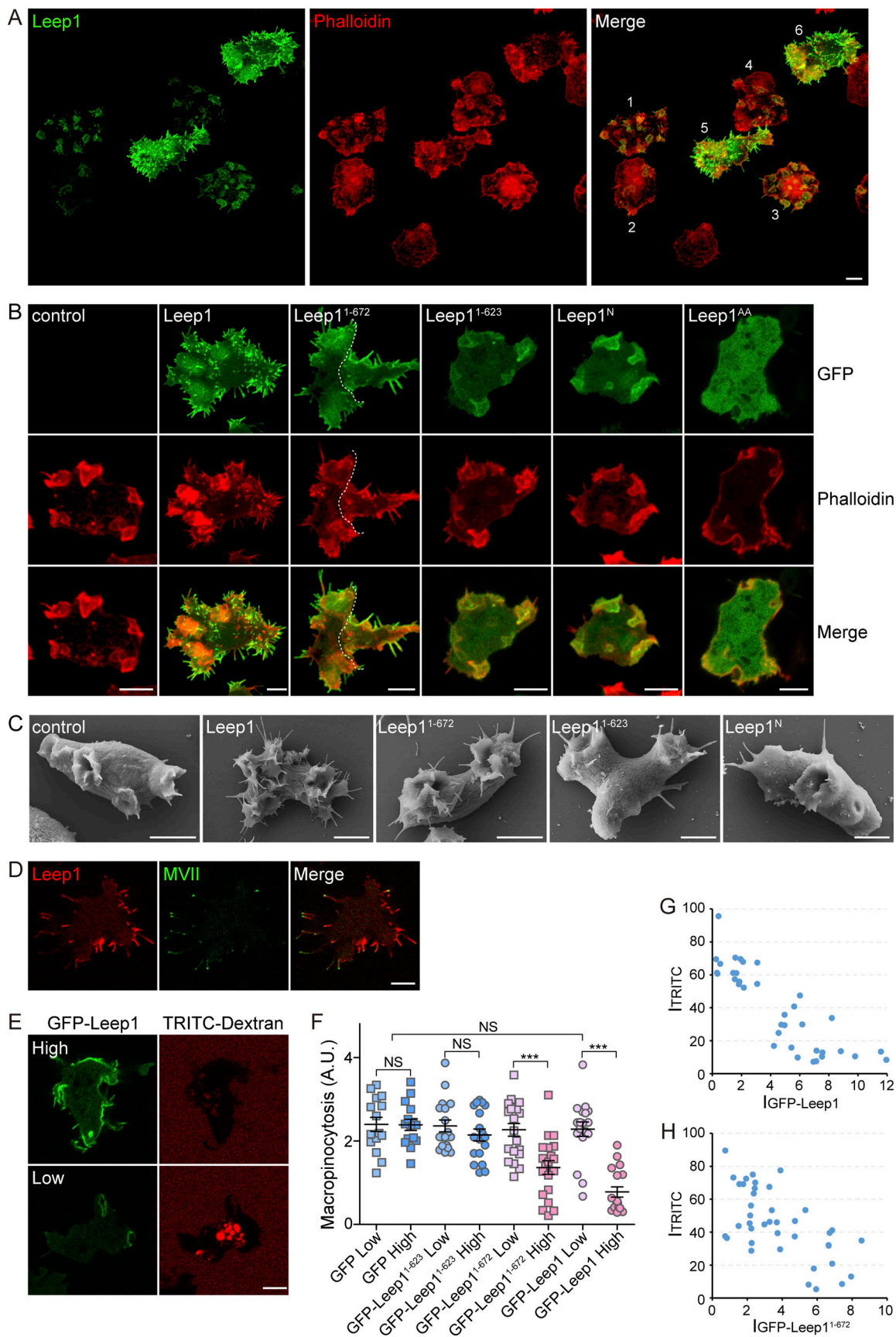


Figure 5. **Leep1 overexpression alters cytoskeletal rearrangement.** (A) Cells expressing low or high levels of GFP-Leep1 (cells 1–4, low expressers; cells 5 and 6, high expressers) were fixed and stained with Alexa Fluor 555–labeled phalloidin. Three-dimensional reconstructions were computed from confocal

sections. **(B)** Cells expressing a control vector (pDM304), Leep1, or truncations and mutation of Leep1 were fixed and stained with Alexa Fluor 555-labeled phalloidin. Three-dimensional reconstructions were computed from confocal sections. Two Leep1¹⁻⁶⁷² cells are separated by a white dashed line. **(C)** Scanning electron micrographs of representative cells expressing a control vector (pDM304) or the full-length or truncated Leep1. **(D)** Colocalization of RFP-Leep1 and GFP-myosin VII (MVII). **(E)** TRITC-dextran uptake in cells expressing high and low levels of GFP-Leep1. Images were acquired 30 min after incubation. **(F)** Quantification of dextran uptake in the high and low expressers. The scatter plots show data points with means and SEM ($n = 15, 15, 18, 18, 20, 20, 18,$ and 18 for the samples listed from left to right). Significance was determined by one-way ANOVA with Dunn's post-test (NS, $P > 0.05$; ***, $P < 0.001$). **(G and H)** Scatter plots showing negative correlation between fluorescence intensity (I) corresponding to GFP-Leep1 (G) or GFP-Leep1¹⁻⁶⁷² (H) and TRITC-dextran (Pearson correlation coefficient = -0.86 , top; -0.63 , bottom). Scale bar = $5 \mu\text{m}$. A.U., arbitrary units.

40.1% similarity to *Dictyostelium* Carmil; 23.7% identity and 35.4% similarity to human CARMIL1), which are known to bind capping proteins (CPs) and induce a conformational change that allosterically decreases actin-capping capacity (Stark et al., 2017). However, further sequence analysis revealed that Leep1 lacks the consensus CP interaction motif (Fig. S3, A and B; Stark et al., 2017). Consistently, Leep1 did not interact with CPs as *Dictyostelium* Carmil (Fig. S3 C; Remmert et al., 2004). The proline-rich domain and verprolin-like and acidic region present in *Acanthamoeba castellanii* and *Dictyostelium* Carmils, which mediate interactions with the Src homology 3 domain of class I myosins and the Arp2/3 complex, respectively, are also either poorly conserved or not relevant to the filopodia-promoting activity of Leep1 (Fig. S3 A; Jung et al., 2001; Stark et al., 2017). In addition, although Leep1 and *Dictyostelium* Carmil both localized to leading-edge structures like macropinocytic cups (Fig. 2 and Fig. S3 D), their responses to stimulation were different. Unlike that of Leep1 (Fig. 3 B), the cAMP-induced translocation of Carmil was abolished by LatA (Fig. S3 E). Thus, despite overall sequence similarity to CARMIL proteins, Leep1 likely functions by a different mechanism.

We sought interacting partners of Leep1 by cross-linking GFP-Leep1 to its neighbors using formaldehyde, which stabilizes weak and transient protein interactions in cells, followed by immunoprecipitation and MS analysis of bound proteins (Fort et al., 2018; Sobczyk et al., 2014). This experiment revealed the pentameric Scar/WAVE complex, a main driver of Arp2/3-mediated branched actin networks (Bear et al., 1998; Davidson and Insall, 2013; Machesky et al., 1999; Miki et al., 1998), as a strong candidate. The complex components, PirA, NapA, and ScrA, were highly enriched in GFP-Leep1 immunocapture but not the GFP control (Table S4). Subsequent coimmunoprecipitation experiment using antibodies to PirA and ScrA confirmed the interaction (Fig. 6 A). Although the Scar complex did not coprecipitate with Leep1 in the absence of cross-linking (Fig. 6 B), the interaction was specific. PirA and ScrA did not precipitate with GFP-Carmil or PHcrac-GFP even upon cross-linking (Fig. 6 A). Similarly, other abundant actin network regulators, such as the Arp2/3 complex and CPs, were not particularly enriched in the GFP-Leep1 immunoprecipitate (Table S4). Notably, a previous study using GFP-NapA as bait also identified Leep1 as an interacting partner (Fort et al., 2018).

Using different truncation or mutation constructs, we performed additional coimmunoprecipitation experiments and activity assays to examine the functional significance of such an interaction. Leep1 interacted with the Scar complex (Fig. 6 A), induced the formation of filopodia when overexpressed (Fig. 5, A–C), and fully rescued the macropinocytosis defect of *leep1*⁻

when expressed at a low level achieved by integrating the GFP-Leep1 expression cassette into the genome as a stable copy via restriction enzyme-mediated integration (REMI; GFP-Leep1^{REMI}; Fig. 6, D and F). In contrast, C-terminally truncated Leep1¹⁻⁶²³ lost the ability to interact with the Scar complex (Fig. 6 A) and failed to promote filopodia formation when overexpressed (Fig. 5, B and C) or rescue the macropinocytosis defect of *leep1*⁻ (Fig. 6, E and G). For Leep1^{AA}, although the interaction with the Scar complex was not affected (Fig. 6 C), it did not induce filopodia formation (Fig. 5 B) or complement the macropinocytosis defect of *leep1*⁻ (Fig. 6 H). These experiments demonstrate that the ability to localize to the proper cellular compartment and interact with the Scar complex underlies the cellular activity of Leep1.

In mammalian and *Dictyostelium* cells, disruption of the activity of Scar/WAVE complex generally leads to reduced macropinocytosis and excessive amounts of filopodia (Beli et al., 2008; Blagg et al., 2003; Litschko et al., 2017; Schaks et al., 2018; Seastone et al., 2001; Steffen et al., 2006), phenotypes also seen with overexpression of Leep1, suggesting that Leep1 may negatively regulate the activity of the complex. To corroborate this hypothesis, we generated PirA-GFP^{REMI}/*pirA*⁻ cells by replacing PirA with a stable copy of PirA-GFP, which largely rescued the growth and macropinocytosis defect of *pirA*⁻ cells. We then deleted *leep1* to generate PirA-GFP^{REMI}/*pirA*⁻*leep1*⁻ cells. This allowed us to compare the behavior of Scar complex in the presence or absence of Leep1.

The Scar complex has been shown to localize at the periphery of macropinocytic cups and the leading edge of pseudopods, where branched F-actin is highly enriched (Veltman et al., 2014; Veltman et al., 2016). Although we could not capture PirA-GFP at the macropinocytic cups due to their rapid deformation and the weak signal intensity in the PirA-GFP^{REMI}/*pirA*⁻*leep1*⁻ cells, we managed to monitor its localization in under-agarose chemotaxing cells (Fig. 6 I and Video 9). We found that PirA-GFP still localized efficiently at pseudopods. Furthermore, the lifetimes of PirA patches were increased, suggesting that PirA-GFP was recruited for a longer duration in the absence of Leep1 (Fig. 6 J). This observation seemed consistent with reduced pseudopod dynamics measured in *leep1*⁻ cells (Fig. 4 J) and an inhibitory function of the interaction between Leep1 and the Scar complex, though a more challenging condition may be required to reveal the consequences of these changes on migration speed and directionality (Fig. 4 I).

Finally, we imaged Leep1 and the Scar complex simultaneously and compared their spatiotemporal pattern in chemotaxing cells placed under agarose. PirA-GFP associated with the leading edge during the progression of a pseudopod and

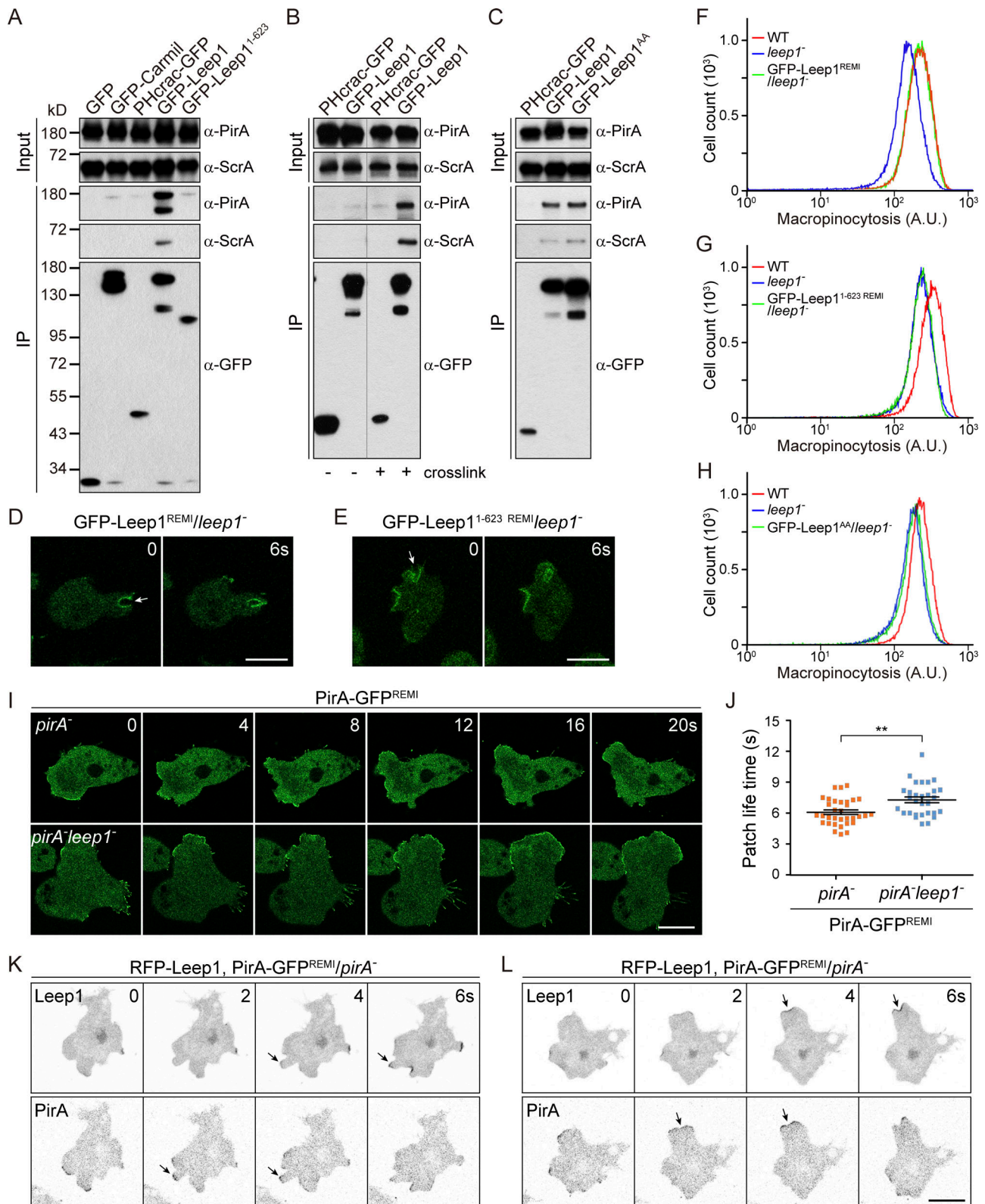


Figure 6. Leep1 interacts with the Scar complex to regulate leading edge activity. (A) Under cross-linking conditions, PirA and ScrA coimmunoprecipitated specifically with GFP-Leep1. **(B)** The interaction between GFP-Leep1 and Scar depended on cross-linking. **(C)** PirA and ScrA coimmunoprecipitated with GFP-Leep1¹⁻⁶²³ REMI. **(D and E)** Time-lapse imaging of cells expressing GFP-Leep1 or GFP-Leep1¹⁻⁶²³ from a stable copy integrated into the genome of *leep1*⁻ via restriction enzyme-mediated integration. Arrows point to macropinocytotic cups. **(F–H)** Flow cytometry analysis of cells incubated with TRITC-dextran for 30 min. Each sample represents ~50,000 cells. **(I)** Time-lapse imaging of PirA-GFP during under-agarose chemotaxis. PirA-GFP was expressed from a stable single copy integrated into the genome. **(J)** Quantification of the average lifetimes of PirA-GFP patches in PirA-GFP^{REMI}/*pirA*⁻ (*n* = 33) and PirA-GFP^{REMI}/*pirA*⁻*leep1*⁻

($n = 30$) cells. **(K and L)** Time-lapse imaging of PirA-GFP^{REMI}/pirA⁻ cells expressing RFP-Leep1 during under-agarose chemotaxis. Arrows point to the accumulation of fluorescent fusion proteins. Graphs in F–H are from one representative experiment out of three independent experiments. Data in J were obtained from two independent experiments, and n represents the number of cells quantified. The scatter plots show data points with means and SEM. Significance was determined by t test with Welch's correction (**, $P < 0.01$). Scale bar = 10 μm . IP, immunoprecipitation; A.U., arbitrary units.

disappeared when it stopped advancing (Fig. 6, K and L; and Video 10). Intriguingly, the emergence of RFP-Leep1 on the same pseudopod was delayed a few seconds and was frequently followed by retraction (Fig. 6 K) or splitting of the pseudopod (Fig. 6 L). Consistent with the previous finding that PIP₃ facilitates the recruitment of Leep1 (Fig. 3, C–I; and Fig. S1), we observed colocalization of RFP-Leep1 and PHcrac-GFP at pseudopods and during their splitting or retraction (Fig. S4, A and B). Together, these observations support our model that PIP₃-mediated recruitment of Leep1 functions to negatively regulate the Scar complex and modulate leading edge dynamics.

Discussion

Targeting components of the signaling and cytoskeleton networks to distinct regions of the plasma membrane and cortex is key to establishing cell polarity. Previous studies in *Dictyostelium* have shown that a panel of molecules localized or activated at the leading or trailing edge of migrating cells exhibits a complementary pattern of distribution when cells also undergo other morphological changes. These findings indicate that a core machinery composed of the same set of polarity regulators may drive morphological changes in general, which ultimately promote diverse cell functions. By exploring the translocation property of known leading and trailing edge molecules in response to chemoattractant stimulation, we developed a proteomics-based approach that enabled a convenient screen for polarity regulators (Fig. 1).

We showed that the method worked effectively for identifying leading edge regulators. We were able to isolate not only well-characterized leading edge-localized molecules, but also molecules, such as GefA and PiaA, that are known to regulate leading edge activities but did not have a polarized distribution when overexpressed as GFP-fusion proteins (Table S3; Chen et al., 1997; Insall et al., 1996). Adding fluorescent tags may disrupt protein function or cause increased background, distorting, or masking of the bona fide localization of a protein. Thus, the proteomics approach may provide a sensitive alternative for analyzing protein localization. In addition, we isolated a number of PIP₃-binding proteins (e.g., PhdA, PhdI, and PkbA) besides PHcrac, indicating that the method was able to capture transient changes in the level of membrane phosphoinositides even though they are known to be unstable after cell lysis.

For trailing edge regulators, the approach could be further optimized. Although several known molecules, such as myosin II and cortexillins, had lower than average translocation scores (Table S3), it was difficult to distinguish them from the majority of nonresponsive molecules because of their small temporal changes. This was partly caused by limited stimuli-induced redistribution of trailing edge proteins in differentiated cells (Swaney et al., 2015). In addition, for reasons we don't fully

understand, the translocation of these proteins was even harder to detect by the membrane fractionation approach. For example, for Pten-GFP, we usually detected no more than a 1.5-fold difference in its abundance in membrane fractions collected at different time points. Undifferentiated cells or cells treated with LatA, which is known to improve the responsiveness of some trailing edge molecules, could be used to help circumvent this problem. This approach may also be applied to other cell types in which signaling or cytoskeleton molecules exhibit synchronous dynamic changes in response to global stimulation (Park et al., 2008; Servant et al., 2000).

Characterization of Leep1 allowed us to obtain intriguing insights into the organization of leading edge structures. Several lines of evidence indicate that phospholipids, primarily PIP₃, mediate the membrane association of Leep1, which in turn modulates leading edge activities by negatively regulating the Scar complex. First, the localization of Leep1 at macropinocytic cups and pseudopods (Fig. 2) depends on its N-terminal lipid binding region and the membrane level of PIP₃ (Fig. 3 and Fig. S1). Second, the amount of Leep1 needs to be fine-tuned for optimal leading edge function. Deletion or overexpression of *leep1* impairs macropinocytosis and alters actin dynamics (Fig. 4 and Fig. 5). Third, Leep1 associates specifically with the Scar complex (Fig. 6, A–C; and Table S4). Although this interaction is weak (Fig. 6, A and B) and not necessary for localizing Leep1 (Fig. S4, C and D), the ability to interact with Scar and to localize to the correct cellular compartment are both needed for the function of Leep1. Truncations or mutations of Leep1 defective in either fail to rescue *leep1*⁻ (Fig. 6, D–H). Finally, the phenotypic resemblance between overexpression of Leep1 (Fig. 5) and disruption of the Scar complex implies Leep1 as a negative regulator of the complex. This is further corroborated by the observation that the absence of Leep1 increases the durations of PirA patches at pseudopods, whereas the emergence of Leep1 is often followed by PirA patch retraction (Fig. 6, I–L).

The ability to interact with both PIP₃ and the Scar complex puts Leep1 in a unique position to control leading edge dynamics. Although PIP₃ and Scar are generally considered to be leading edge-localized, previous studies have demonstrated the complexity of their spatial organization (Hoeller and Kay, 2007; Veltman et al., 2014; Veltman et al., 2016). Intriguing, high concentrations of PIP₃ do not seem to overlap with the Scar complex in *Dictyostelium*. During macropinocytosis, self-organized patches of PIP₃ somehow recruit the Scar complex to their periphery; the region labeled with PIP₃ remains static during cup formation, whereas the Scar complex-containing region moves outward and drives cup closure. Consistently, we observed an accumulation of ArpC4 at the periphery of Leep1-labeled macropinocytic cups (Fig. S4, E and F). In migrating cells, PIP₃ also seems to hinder Scar-mediated pseudopod progression in some cases (Veltman et al., 2014). By localizing to regions with

high PIP₃ and negatively regulating the Scar complex, Leep1 may help spatially restrict the activity of the complex.

The detailed mechanism of how Leep1 regulates the Scar complex awaits further investigation. It likely involves the C terminus of Leep1, which is necessary for binding with Scar, as well as the N-terminal PH domain-like region, which is required for membrane localization. Evidence indicates that the importance of the N-terminal region goes beyond lipid binding; swapping it with other phospholipid-binding domains, even those with similar binding preference, abolished the function of Leep1 (Fig. S4, G and H). For example, when the N-terminal region of Leep1 (between aa 17 and 140), which contains the putative PH domain, was replaced with the PH domain of PkgE (Bloomfield et al., 2015), the chimeric protein failed to rescue the macropinocytosis defect of *leep1*⁻ even though it localized to macropinocytotic cups like Leep1 (Fig. S4, G and H). As Leep1 exhibited more extensive colocalization with PIP₃ than the Scar complex, it will be interesting to investigate whether Leep1 has functions in addition to interactions with Scar.

The mild phenotypes of *leep1*⁻ in macropinocytosis and migration may reflect the existence of parallel or redundant pathways. A previous study identified a different negative regulator of the Scar/WAVE complex (Fort et al., 2018). CYRI is an evolutionarily conserved protein that binds activated Rac1 via a domain shared with CYFIP (homologue of PirA in mammalian cells), thereby limiting Rac1- and Scar/WAVE-mediated actin polymerization. Though the effect of this mechanism on macropinocytosis has not been investigated, deletion of *cyri* leads to a stronger defect in cell migration than deletion of *leep1*. In addition, Leep1 and CYRI differ in their localization mechanisms. Leep1 localizes to the plasma membrane by interacting with PIP₃, whereas CYRI localizes to the plasma membrane via myristoylation (Fort et al., 2018). Further studies are needed to determine whether Leep1 and CYRI work together to modulate Scar activity. It is also possible that homologues of Leep1 can substitute for its function in *leep1*⁻. In addition to Carmil (Fig. S3), there are eight uncharacterized proteins in *Dictyostelium* that share extensive sequence similarity with Leep1 in the N-terminal and LRR regions (~22–25% identity and 41–45% similarity). However, we found that none of these proteins contain domains that are similar to the C terminus of Leep1, which is required for its function (Fig. 6, D–G), and none localized specifically to macropinocytotic cups or pseudopods when expressed as GFP-fusion proteins. Thus, whether there exist functional homologues of Leep1 remains an open question. Considering that deletion of the Scar complex causes only partial defects in cell migration and macropinocytosis (Blagg et al., 2003; Litschko et al., 2017; Schaks et al., 2018; Seastone et al., 2001), other actin regulators may also contribute to the remaining activities seen in the *leep1*⁻ cells.

In conclusion, we developed a proteomics-based approach to comprehensively identify polarly distributed molecules. Through this approach, we identified Leep1 as a novel polarity regulator, which modulates leading edge activities by binding with PIP₃ and negatively regulating the Scar/WAVE complex. It will be of great interest in future studies to investigate whether

the spatiotemporal organization of PIP₃ and Scar/WAVE domains is conserved in pseudopod and macropinocytotic cup morphogenesis in higher eukaryotic cells.

Materials and methods

Cell growth and differentiation

WT cells were derived from the Ax2 (Ka) axenic strain provided by the Robert Kay laboratory (MRC Laboratory of Molecular Biology, London, UK; Bloomfield et al., 2008). All gene deletion cell lines were generated in Ax2. WT and gene deletion cells were cultured in HL5 medium (Formedium; cat# HLF3) supplemented with antibiotics. Cells carrying expression constructs were maintained in HL5 containing G418 (10–20 µg/ml) or hygromycin B (50 µg/ml). Development on bacteria lawn, on non-nutrient agar, or with cAMP pulses was performed as described before (Cai et al., 2014).

Gene disruption and plasmid construction

To make knockout constructs for *leep1* and *Dd5P4* deletion, a blasticidin S resistance (BSR) cassette was inserted into pBlueScript II SK+ to generate pBlueScript-BSR. 5' and 3' arms were PCR-amplified from genomic DNA with primers listed in Table 1 and cloned upstream and downstream of the BSR cassette, respectively. The *pirA*⁻ knockout construct was described before (Schaks et al., 2018). The resulting disruption cassette was PCR-amplified and electroporated into Ax2. Gene disruption was confirmed by resistance to blasticidin (10 µg/ml), PCR, and Southern or Western Blotting. To generate *pirA*⁻*leep1*⁻ cells, the BSR cassette was removed from *pirA*⁻ cells by transformation with a Cre recombinase expression plasmid, pDEX-NLS-Cre (Faix et al., 2004), and selection with 20 µg/ml G418. The *leep1* gene was then disrupted in *pirA*⁻ cells.

To generate constructs expressing GFP- or RFP-fusion proteins, DNA fragments encoding full-length or truncations of Leep1, Carmil, PH_{PkgE}, ArpC4, mouse GRP1, or human TAPP1 were PCR-amplified using primers listed in Table 1 and cloned into pDM317, pDM323, pDM449, or pDM451 (Veltman et al., 2009) containing a multiple cloning site. The sequence encoding cPH×3 was *Dictyostelium* codon-optimized and cloned into pDM317 or pDM449. To generate GFP-Leep1^{AA}, the lysine residue at position 28 and arginine residue at position 39 were mutated to alanines. To generate constructs expressing GFP-tagged chimeric proteins presented in Fig. S4 G, we replaced the N terminus of Leep1 between aa 1 and 140 or 17 and 140 with the PH domain of PkgE (aa 1–100) or CRAC (aa 1–126).

Constructs for integrating GFP-Leep1 and GFP-Leep1^{1–623} into the genome by REMI were made by removing the sequence between NgoMIV and HindIII in the vector backbone. The resulting fragment was gel-purified, blunted using the NEB Quick Blunting kit, and religated. The PirA-EGFP^{REMI} construct was described before (Schaks et al., 2018). For genomic integration, these constructs were linearized with XhoI and electroporated into the appropriate cells together with XhoI. Clones were selected with G418. Stability of expression was examined by Western blotting or imaging after single-cell expansion with bacteria for multiple generations.

Table 1. Primers used in this study

Expression in Dictyostelium cells		
Usage	Plasmid backbone	Sequence, 5'-3'
GFP-Leep1	pDM317	F: GGGGATCCATGTCATCCGAATTATCTACTGGTG R: GGTCTAGAATATTCTGGAGGTGGTGGCATTCTA
GFP-Leep1 ¹⁻⁸⁵⁵	pDM317	F: CTAAGTCTAGAGTTCATCCGAATTATCTACTGGT R: CTAGTCGACTTACATTCTATTTTCGTCTTCATATTG
GFP-Leep1 ¹⁻⁷⁶⁴	pDM317	F: CTAAGTCTAGAGTTCATCCGAATTATCTACTGGT R: CTAGTCGACTTAACTATAGTCATAAGTTTCTTGTGG
GFP-Leep1 ¹⁻⁷⁵¹	pDM317	F: CTAAGTCTAGAGTTCATCCGAATTATCTACTGGT R: CTAGTCGACTTATTGTTGATAATGATTGCATAAACATC
GFP-Leep1 ¹⁻⁷³⁶	pDM317	F: CTAAGTCTAGAGTTCATCCGAATTATCTACTGGT R: CTAGTCGACTTAAAGCATAAGTTGAAGGTGATGGTGA
GFP-Leep1 ¹⁻⁶⁷²	pDM317	F: CTAAGTCTAGAGTTCATCCGAATTATCTACTGGT R: CTAGTCGACTTGAGAGACAAGTTTGAACATCAG
GFP-Leep1 ¹⁻⁶²³	pDM317	F: CTAAGTCTAGAGTTCATCCGAATTATCTACTGGT R: CTAGTCGACTTAGGTTGTAAAGTTCTTTTCATAGC
GFP-Leep1 ^N	pDM317	F: GGGGATCCATGTCATCCGAATTATCTACTGGTG R: GGTCTAGATTGGTTCTCTTTCAAGGCGTCAC
GFP-Leep1 ^M	pDM317	F: GGGGATCCTTGGCCGACGTTTCCATCATAAT R: GGTCTAGAAAGGTACGATTGGTTGTGAAAG
GFP-Leep1 ^C	pDM317	F: GGGGATCCCGTACCCTTATCGATATACCAGTAC R: GGTCTAGAAATATTCTGGAGGTGGTGGCATTCTA
GFP-Leep1 ^{K28AR39A}	pDM317	Insert 1 F: CTATCTAGAAATGTCATCCGAATTATCTACTGGT Insert 1 R: GCATCTTGAACAACATCTTTTTTATTGTTTTTG Insert 2 F: GATGTTGTTCAAGATGCTCTTTTTG Insert 2 R: CTAGTCGACATATTCTGGAGGTGGTGGCATTCTATTTTC
RFP-Leep1	pDM449	F: GGGGATCCATGTCATCCGAATTATCTACTGGTG R: GGTCTAGAATATTCTGGAGGTGGTGGCATTCTA
GFP-Carmil	pDM317	F: GGGGATCCATGTCAGAAGAAATATACCAAATG R: GGACTAGTATTTTCGGTCCGGTGGTCTTGGTCTTC
GFP-PH _{pkGE}	pDM317	F: CCTCTAGAAATGGCAGATAAACAAGGATTTTAAATT R: CCGTCGACTGTAGATCTTTAAGTTTATTTAAATT
GFP-ArpC4	pDM317	F: GGGGTACCATGTCCACAGCTCAAGTTCCATATTTAAATTG R: CGAGCGCCCGCAGCAAAGTTCTTTAAGTATTAGAAGCAAC
TAPP1-GFP	pDM323	F: CCGGAGCTCATGCCTTATGTGGATCGTCAG R: CTAGCTAGCCACGTCCTACTGACCGGAAGGC
TAPP1-RFP	pDM451	F: CCGGAGCTCATGCCTTATGTGGATCGTCAGAATC R: CTAGCTAGCCACGTCCTACTGACCGAAGGCTCGC
PH _{GRP1} -GFP	pDM323	F: CTATCTAGAAATGTATGAAAGTATCAAGAAATGAGCCG R: CTAGTCGACTTTCTTATTGGCAATCCTCTTTTC
Generation of knockout cells		
<i>leep1</i> knockout	pBluescript-BSR	Insert 1 F: GGGGTACCATGTCATCCGAATTATCTACTGGTG Insert 1 R: GCGTCGACAATAATTCTATGAAATGCATTAATTA Insert 2 F: CGGGGATCCGATCAACAACAATGAAGACG Insert 2 R: CCGGCGGCCGCTTGTGAAACATGAATTGTACC

Table 1. Primers used in this study (Continued)

Expression in <i>Dictyostelium</i> cells		
Usage	Plasmid backbone	Sequence, 5'-3'
Dd5P4 knockout	pBluescript-BSR	Insert 1 F: CACGGTACCGATTAACAAAATGAAACGCAACTTTTC
		Insert 1 R: GAGAAGCTTCTGTATTTTGAATATCACCCATTG
		Insert 2 F: CGCGGATCCGATGCTACAACCTGTAAAAAGAAAGCTG
		Insert 2 R: CCGGCGGCCGCGTTGAAAAAGACATTAATTGGTTTCTC

All primer sequences are given in 5' to 3' direction, and each primer is designated as forward (F) or reverse (R).

Peripheral membrane protein isolation and MS analysis

Cells expressing PHcrac-GFP were developed with cAMP pulses for 3–4 h, basalated with caffeine, and washed with development buffer (DB; 5 mM Na₂HPO₄, 5 mM KH₂PO₄, 2 mM Mg₂SO₄, and 0.2 mM CaCl₂) as described before (Cai et al., 2010). Cells were resuspended in DB at 8 × 10⁷ cells/ml and stimulated with 10 μM cAMP. At each time point, 200 μl aliquots of cells were quickly mixed with equal volume of TM buffer (20 mM Tris pH 8.0, 2 mM MgSO₄), then lysed through two layers of 5-μm filter membranes (Millipore). Lysed samples were immediately mixed with 2 ml ice-cold PM buffer (5 mM Na₂HPO₄, 5 mM KH₂PO₄, 2 mM MgSO₄, pH 6.5), centrifuged at 350 × g at 4°C to remove debris and intact cells, and then at 12,000 × g for 5 min. Pelleted membrane fractions were resuspended with 100 mM Na₂CO₃ (pH 11.3) and homogenized, then centrifuged at 100,000 × g for 60 min at 4°C. The supernatants were collected as peripheral membrane protein fractions and concentrated by TCA precipitation. The precipitated pellets were dissolved in 100 mM Tris, pH 8.5, and 8 M urea. Protein concentrations were determined by BCA protein assay (Bio-Rad).

Equal amounts of proteins were separated by SDS-PAGE and stained using the Colloidal Blue Staining Kit (Thermo Fisher Scientific). Each gel lane was cut into four slices and digested with trypsin. Liquid chromatography–tandem MS analysis of the resulting peptides was conducted on a Q Exactive mass spectrometer (Thermo Fisher Scientific) interfaced with an Easy-nLC1000 liquid chromatography system (Thermo Fisher Scientific). Peptides were loaded on a precolumn (75 μm internal diameter, 6 cm long, packed with ODS-AQ 120 Å–10 μm beads from YMC Co., Ltd.) and separated on an analytical column (75 μm internal diameter, 13 cm long, packed with Luna C18 1.8 μm 100 Å resin from Welch Materials) using an 0%–30% (vol/vol) acetonitrile gradient over 120 min at a flow rate of 200 nl/min, with 0.1% (vol/vol) formic acid added to the mobile phase throughout. The top 15 most intense precursor ions from each full scan (resolution 70,000) were isolated for HCD MS2 (resolution 17,500; NCE 27), with a dynamic exclusion time of 45 s. Precursors with unassigned charge states or charge states of 1+, 8+, or >8+ were excluded. Peptides and proteins were identified from the MS data using the database searching engine pFind 3.1 (<http://pfind.ict.ac.cn/>) against the UniProt *Dictyostelium discoideum* protein database (UP000002195_44689; <https://www.uniprot.org/proteomes/UP000002195>). The filtering criteria were a 1% false discovery rate at both the peptide level and the protein level;

precursor mass tolerance, 20 ppm; fragment mass tolerance, 20 ppm; and peptide length, 6–100 aa.

Lipid dot blot assay and lipid-coated agarose bead pull-down assay

Lipid dot blot assay was performed as described before (Swaney et al., 2015) with minor modifications. Cells expressing GFP-Leep1 were washed, resuspended in DB at 2 × 10⁷ cells/ml, and starved without cAMP pulses for 3 h. Starved cells were lysed by lysis buffer (10 mM NaPi, pH 7.0, 150 mM NaCl, 0.5% NP-40, and complete EDTA-free protease inhibitor; Roche) at 5 × 10⁷ cells/ml. Lysates were centrifuged at 10,000 × g for 10 min at 4°C. The supernatants were mixed with equal volume of buffer (10 mM NaPi, pH 7.0, 150 mM NaCl, and protease inhibitor) and incubated with preblocked PIP strips (Echelon) at 4°C for 3 h. PIP strips were washed and incubated sequentially with anti-GFP antibody and HRP-conjugated anti-mouse second antibody. Signal was detected by chemiluminescence using ECL Western blotting detection reagent (GE Healthcare).

For the lipid-coated bead pull-down assay, cells expressing GFP-tagged protein were washed and starved in DB at 2 × 10⁷ cells/ml for 3 h. Starved cells were resuspended at 8 × 10⁷/ml in binding buffer without detergent (10 mM Hepes, pH 7.2–7.4, 150 mM NaCl, and protease inhibitor) and lysed through 5-μm filter membranes. Lysates were centrifuged at 15,000 rpm for 10 min at 4°C. NP-40 was added to the supernatants to a final concentration of 0.25%. Cell lysates were then incubated with prewashed lipid-coated beads (Echelon) at 4°C for 1–3 h. Beads were washed five times with binding buffer with NP-40. Samples were eluted with SDS loading buffer and subjected to SDS-PAGE.

Macropinocytosis assay

For monitoring TRITC-dextran uptake, cells seeded in an 8-well coverslip chamber (Lab-Tek; NalgenNunc) were incubated with HL5 supplemented with 1 mg/ml TRITC-dextran (Sigma-Aldrich; cat# T1162). At selected time points, images were acquired on a Zeiss 880 inverted microscope with a 63 ×/1.4 oil-immersion objective. Fluorescence intensity per cell was quantified by ImageJ. Macropinocytosis dynamics was recorded in WT and *leep1*⁻ cells expressing PHcrac-GFP by time-lapse videos taken at 2- or 3-s intervals. To quantify the rate of macropinocytosis, cells were tracked and included in the analysis only if they remained within the field for at least 5 min. Ruffle size was determined by measuring the length of PHcrac-GFP patch

with the freehand line tool in ImageJ. For flow cytometry analysis, cells seeded in 6-well plates were incubated with HL5 supplemented with 0.5 mg/ml TRITC-dextran for 30 min. Cells were washed with ice-cold HL5 and KK2 (6.5 mM KH_2PO_4 and 3.8 mM K_2HPO_4 , pH 6.2) and resuspended in KK2 containing 5 mM EDTA. The total fluorescence intensity per cell was determined by a BD Biosciences Influx flow cytometer. Data were analyzed by FlowJo.

Phagocytosis assay

Phagocytosis of TRITC-labeled yeast particles was quantified following a standard protocol (Junemann et al., 2016). In brief, vegetative cells were grown in a shaken suspension at 150 rpm in HL5 and adjusted to a density of 2×10^6 cells/ml. TRITC yeast was added at a sixfold excess. Aliquots of 1 ml were taken at each time point and incubated on ice for 3 min with 100 μl of Trypan Blue solution (2 mg/ml in 20 mM citrate and 150 mM NaCl, pH 4.5). Cells were then pelleted, washed once with ice-cold Sørensen buffer (14.6 mM KH_2PO_4 and 2.0 mM Na_2HPO_4 , pH 6.1), and resuspended in 1 ml of Sørensen buffer for immediate measurement in a Tecan Spark fluorescence spectrophotometer (544-nm excitation and 574-nm emission). To image phagocytosis, WT and *leep1⁻* cells were seeded in a coverslip chamber in KK2 with a 10-fold excess of TRITC-labeled yeast particles. After 60 min, yeast particles that were not internalized were quenched by Trypan Blue. Confocal images were taken to count the number of internalized yeast particles.

Bacteria phagocytosis assay was performed as described before (Junemann et al., 2016). Briefly, WT and *leep1⁻* cells were washed and resuspended in DB at 2×10^6 cells/ml. After shaking at 150 rpm for 30 min, the cells were mixed with an equal volume of bacteria suspension. At the indicated time points, cell were pelleted for 1 min at $700 \times g$, and the OD₆₀₀ of the supernatants containing bacteria was measured.

Imaging

To image the localization of fluorescent proteins in vegetative cells, 10^5 cells were plated in an 8-well coverslip chamber and allowed to adhere. Images were taken on a Zeiss 880 inverted microscope equipped with a 40 \times /0.95 or 63 \times /1.4 oil-immersion objective.

To image protein translocation in response to cAMP stimulation, cells developed with cAMP pulses for 4 h were plated in an 8-well coverslip chamber and allowed to adhere for at least 15 min. 1 μM cAMP was added for stimulation. Cells were pre-treated for 10 min with 5 μM LatA (Enzo Life Sciences; cat# BML-T119-0100) or 45 min with 60 μM LY294002 (Cayman Chemical; cat# 70920) before the addition of cAMP. To image GFP-Leep1 translocation in response to folic acid stimulation, 10^5 vegetative cells were plated in an 8-well coverslip chamber in HL5. After the cells settled, HL5 was replaced with DB. 200–500 μM folic acid was added for stimulation after \sim 30 min.

For phalloidin staining, cells were seeded in coverslip chamber overnight in HL5. Cells were fixed for 8 min with 2% paraformaldehyde and 0.08% glutaraldehyde in KK2, permeabilized for 8 min with the addition of 0.2% TX-100, quenched in PBS containing 20 mM glycine, and washed with KK2. Cells were stained with TRITC-conjugated phalloidin

(Sigma-Aldrich; cat# P1951) for 30 min. Three-dimensional stacks (100 nm z-step) were captured on a Zeiss 880 inverted microscope equipped with a 63 \times /1.4 oil-immersion objective.

Scanning electron microscopy

Cells were plated on an ethanol-washed glass coverslip overnight in HL5. To fix the cells, HL5 was replaced with 1% OsO_4 in KK2 for \sim 5 s, and then replaced with 2% glutaraldehyde in KK2. Fixation in glutaraldehyde was continued for 2 h at room temperature and overnight at 4°C. Fixed cells were washed with PBS, progressively dehydrated through an ethanol series of 20–100%, and then critical point-dried and gold-coated. Images were taken on a Hitachi SU8010 Ultra-High Resolution (1.0 nm) Scanning Electron Microscope.

Migration assays

For random motility assay, 2×10^5 vegetative cells were plated in a 2-well coverslip chamber in HL5 and allowed to attach for 4 h. Images were acquired at 20-s intervals with phase illumination on a Zeiss 880 inverted microscope equipped with a 20 \times /0.8 objective.

For micropipette chemotaxis assay, differentiated cells were seeded in a 1-well coverslip chamber filled with DB and allowed to adhere for 15–20 min. A micropipette (Eppendorf Femtotip II) filled with 1 μM cAMP was placed into the field of view using a manipulator (Eppendorf Injectman and Femtojet). Cell movement was recorded at 10-s intervals using a Zeiss 880 inverted microscope equipped with a 40 \times /0.95 oil-immersion objective.

Under-agarose folate chemotaxis assay was performed as described before (Tweedy et al., 2016; Woznica and Knecht, 2006). For experiments presented in Fig. 2 I; Fig. 6, I, K, and L; Fig. S1 A; Fig. S2 I; and Fig. S4, A–C, 5 ml of 0.5% SeaKem GTG agarose melted in LoFlo medium (Formedium) was poured into a 50-mm glass-bottom dish (MatTek Corp.) pretreated with 1% BSA in LoFlo. After setting of the agarose, two troughs (3 mm wide and 5 mm apart) were cut. One trough was filled with vegetative cells resuspended in LoFlo (2×10^6 cells/ml) and the other with 1 mM (Fig. 2 I; Fig. 6, I, K, and L; Fig. S1 A; and Fig. S4, A–C) or 25 μM (Fig. S2 I) folic acid. For experiments presented in Fig. 4, I and J, 5 ml of agarose containing 10 μM folic acid was poured into a glass-bottom dish. After setting of the agarose, one trough 5 mm wide was cut and filled with vegetative cells. Cells were allowed to migrate for 4–9 h. Images were acquired at 20-s intervals with a 10 \times /0.45 phase objective (Fig. 4 I and Fig. S2 I) or at 2- or 3-s intervals with a 40 \times /0.95 or 63 \times /1.4 oil-immersion objective on a Zeiss 880 inverted microscope or a Zeiss 980 Airyscan confocal microscope equipped with a Fastscan detector. To quantify migration parameters, including the accumulated distance, Euclidean distance, velocity, directness, and forward migration index, cells were tracked using manual tracking plugin of FIJI ImageJ (<https://fiji.sc/>) and analyzed using Ibidi chemotaxis tool software. The pseudopod split frequency was analyzed from videos and manually quantified frame by frame.

Immunoprecipitation

GFP-trap with formaldehyde cross-linking was performed as described before (Fort et al., 2018). Briefly, GFP expressing cells

were lysed by lysis/cross-linking buffer. Formaldehyde was quenched on ice using 1.75 M Tris, pH 8.0. Samples were centrifuged at $22,000 \times g$ for 4 min at 4°C. The pellets were washed sequentially with quenching buffer, wash buffer A, and wash buffer B. After the final wash, the pellets were re-suspended using 1 ml of ice-cold radioimmunoprecipitation assay buffer and incubated for 1 h at 4°C with gentle agitation. Supernatants were mixed with GFP-Trap beads (ChromoTek) and rotated for 1 h at 4°C. Beads were washed three times with 50 mM Tris, pH 8.0, 150 mM NaCl, and 5 mM EDTA, followed by one wash with 10 mM Tris, pH 8.0. Samples were eluted after incubation with 2 × SDS loading buffer and heated for 10 min at 70°C before being subjected to SDS-PAGE.

For immunoprecipitation assay, in the absence of cross-linking, cells expressing GFP-fusion proteins were lysed by ice-cold lysis buffer (10 mM NaPi, pH 7.2, 100 mM NaCl, 0.5% NP-40, 10% glycerol, 1 mM NaF, 0.5 mM Na₃VO₄, and protease inhibitor) and incubated for 5 min on ice. Lysates were centrifuged at $22,000 \times g$ for 5 min at 4°C. The supernatants were incubated with GFP-Trap beads for 30 min at 4°C. Beads were washed three times with lysis buffer. Samples were eluted with SDS loading buffer and subjected to SDS-PAGE.

Immunoblotting

Western blotting was performed as described before (Cai et al., 2010). Anti-GFP antibody from Roche (11814460001) was used to detect PHcrac-GFP and GFP-Leep1. Anti-CP antibody was purchased from the Developmental Studies Hybridoma Bank (135-409-16). Anti-ScrA and anti-PirA antibodies were from R. Insall's laboratory (Ibarra et al., 2006).

Online supplemental material

Fig. S1 shows the regulation of membrane association of Leep1. Fig. S2 shows the generation and characterization of *leep1* knockout cells. Fig. S3 shows the sequence and activity of *Dictyostelium* Carmil. Fig. S4 shows the analysis of the localization and function of Leep1. Video 1, Video 2, and Video 3 show the localization of GFP-Leep1 in response to cAMP stimulation and during macropinocytosis or chemotaxis. Video 4 shows colocalization of GFP-Leep1 and RFP-LimEΔcoil. Video 5 shows the dynamics of PHcrac-GFP in WT and *leep1*⁻ cells. Video 6 shows under-agarose chemotaxis of WT and *leep1*⁻ cells. Video 7 shows the trajectory of WT or *leep1*⁻ cells expressing GFP-ArpC4 during under agarose chemotaxis. Video 8 shows overexpression of full-length or truncated Leep1. Video 9 shows PirA-GFP^{REMI}/*pirA*⁻ or PirA-GFP^{REMI}/*pirA*⁻*leep1*⁻ cells migrating along folate gradients under agarose. Video 10 shows PirA-GFP^{REMI}/*pirA*⁻ cells expressing RFP-Leep1 migrating along folate gradients under agarose. Table S1, Table S2, and Table S3 show MS analysis of peripheral membrane proteins, and Table S4 shows proteomic identification of Leep1-binding proteins.

Acknowledgments

We thank Dr. Peter Devreotes (Johns Hopkins University, Baltimore, MD) for providing PHcrac-GFP plasmid and *pten*⁻ cells; Dr. Robert Kay (MRC Laboratory of Molecular Biology, London,

UK) for PH_{pkGE}-mCherry plasmid, pDM vectors, and Ax2 cells; Dr. Margaret Titus (University of Minnesota, Minneapolis, MN) for GFP-Myo7 plasmid; Dr. Richard Firtel (University of California, San Diego, San Diego, CA) for *pi3k1-2*⁻ cells; Dr. Miho Iijima (Johns Hopkins University, Baltimore, MD) for GFP-Pten plasmid; and Dr. Xiaochen Wang (Institute of Biophysics, Chinese Academy of Sciences, Beijing, China) for TAPP1 plasmid. We thank the proteomics core facility in Tsinghua University for MS analysis and the Center for Biological Imaging at the Institute of Biophysics for assistance with data collection.

This work was supported by grants from the Ministry of Science and Technology of the People's Republic of China (2016YFA0500202 to H. Cai), the Strategic Priority Research Program of the Chinese Academy of Sciences (XDB37020304 to H. Cai), and the National Natural Science Foundation of China (31770894 to H. Cai and 31872828 to Y. Yang).

The authors declare no competing financial interests.

Author contributions: H. Cai and Y. Yang designed research, analyzed data, and wrote the manuscript; Y. Yang, D. Li, X. Chao, and H. Cai collected the data; Y. Yan, M. Dong, and L. Li provided support for MS experiments; and S.P. Singh, P. Thomason, and R.H. Insall provided essential reagents and advice.

Submitted: 21 October 2020

Revised: 23 March 2021

Accepted: 21 April 2021

References

- Artemenko, Y., T.J. Lampert, and P.N. Devreotes. 2014. Moving towards a paradigm: common mechanisms of chemotactic signaling in Dictyostelium and mammalian leukocytes. *Cell. Mol. Life Sci.* 71:3711–3747. <https://doi.org/10.1007/s00018-014-1638-8>
- Bear, J.E., J.F. Rawls, and C.L. Saxe III. 1998. SCAR, a WASP-related protein, isolated as a suppressor of receptor defects in late Dictyostelium development. *J. Cell Biol.* 142:1325–1335. <https://doi.org/10.1083/jcb.142.5.1325>
- Beli, P., D. Mascheroni, D. Xu, and M. Innocenti. 2008. WAVE and Arp2/3 jointly inhibit filopodium formation by entering into a complex with mDia2. *Nat. Cell Biol.* 10:849–857. <https://doi.org/10.1038/ncb1745>
- Bentley, M., and G. Banker. 2016. The cellular mechanisms that maintain neuronal polarity. *Nat. Rev. Neurosci.* 17:611–622. <https://doi.org/10.1038/nrn.2016.100>
- Blagg, S.L., M. Stewart, C. Sambles, and R.H. Insall. 2003. PIR121 regulates pseudopod dynamics and SCAR activity in Dictyostelium. *Curr. Biol.* 13:1480–1487. [https://doi.org/10.1016/S0960-9822\(03\)00580-3](https://doi.org/10.1016/S0960-9822(03)00580-3)
- Bloomfield, G., Y. Tanaka, J. Skelton, A. Ivins, and R.R. Kay. 2008. Widespread duplications in the genomes of laboratory stocks of Dictyostelium discoideum. *Genome Biol.* 9:R75. <https://doi.org/10.1186/gb-2008-9-4-r75>
- Bloomfield, G., D. Traynor, S.P. Sander, D.M. Veltman, J.A. Pachebat, and R.R. Kay. 2015. Neurofibromin controls macropinocytosis and phagocytosis in Dictyostelium. *eLife.* 4:e04940. <https://doi.org/10.7554/eLife.04940>
- Brzeska, H., H. Koech, K.J. Pridham, E.D. Korn, and M.A. Titus. 2016. Selective localization of myosin-I proteins in macropinosomes and actin waves. *Cytoskeleton (Hoboken)*. 73:68–82. <https://doi.org/10.1002/cm.21275>
- Buckley, C.M., H. Pots, A. Gueho, J.H. Vines, C.J. Munn, B.A. Phillips, B. Gilsbach, D. Traynor, A. Nikolaev, T. Soldati, et al. 2020. Coordinated Ras and Rac Activity Shapes Macropinocytic Cups and Enables Phagocytosis of Geometrically Diverse Bacteria. *Curr. Biol.* 30:2912–2926.e5. <https://doi.org/10.1016/j.cub.2020.05.049>
- Buczynski, G., B. Grove, A. Nomura, M. Kleve, J. Bush, R.A. Firtel, and J. Cardelli. 1997. Inactivation of two Dictyostelium discoideum genes, DdPIK1 and DdPIK2, encoding proteins related to mammalian phosphatidylinositol 3-kinases, results in defects in endocytosis, lysosome

- to postlysosome transport, and actin cytoskeleton organization. *J. Cell Biol.* 136:1271–1286. <https://doi.org/10.1083/jcb.136.6.1271>
- Cai, H., S. Das, Y. Kamimura, Y. Long, C.A. Parent, and P.N. Devreotes. 2010. Ras-mediated activation of the TORC2-PKB pathway is critical for chemotaxis. *J. Cell Biol.* 190:233–245. <https://doi.org/10.1083/jcb.201001129>
- Cai, H., M. Katoh-Kurasawa, T. Muramoto, B. Santhanam, Y. Long, L. Li, M. Ueda, P.A. Iglesias, G. Shaulsky, and P.N. Devreotes. 2014. Nucleocytoplasmic shuttling of a GATA transcription factor functions as a development timer. *Science.* 343:1249531. <https://doi.org/10.1126/science.1249531>
- Campanale, J.P., T.Y. Sun, and D.J. Montell. 2017. Development and dynamics of cell polarity at a glance. *J. Cell Sci.* 130:1201–1207. <https://doi.org/10.1242/jcs.188599>
- Charest, P.G., Z. Shen, A. Lakoduk, A.T. Sasaki, S.P. Briggs, and R.A. Firtel. 2010. A Ras signaling complex controls the RasC-TORC2 pathway and directed cell migration. *Dev. Cell.* 18:737–749. <https://doi.org/10.1016/j.devcel.2010.03.017>
- Chen, M.Y., Y. Long, and P.N. Devreotes. 1997. A novel cytosolic regulator, Pianissimo, is required for chemoattractant receptor and G protein-mediated activation of the 12 transmembrane domain adenylyl cyclase in Dictyostelium. *Genes Dev.* 11:3218–3231. <https://doi.org/10.1101/gad.11.23.3218>
- Chen, C.L., Y. Wang, H. Sesaki, and M. Iijima. 2012. Myosin I links PIP3 signaling to remodeling of the actin cytoskeleton in chemotaxis. *Sci. Signal.* 5:ra10. <https://doi.org/10.1126/scisignal.2002446>
- Chiou, J.G., M.K. Balasubramanian, and D.J. Lew. 2017. Cell Polarity in Yeast. *Annu. Rev. Cell Dev. Biol.* 33:77–101. <https://doi.org/10.1146/annurev-cellbio-100616-060856>
- Clow, P.A., and J.G. McNally. 1999. In vivo observations of myosin II dynamics support a role in rear retraction. *Mol. Biol. Cell.* 10:1309–1323. <https://doi.org/10.1091/mbc.10.5.1309>
- Davidson, A.J., and R.H. Insall. 2013. SCAR/WAVE: A complex issue. *Commun. Integr. Biol.* 6:e27033. <https://doi.org/10.4161/cib.27033>
- Davidson, A.J., C. Amato, P.A. Thomason, and R.H. Insall. 2018. WASP family proteins and formins compete in pseudopod- and bleb-based migration. *J. Cell Biol.* 217:701–714. <https://doi.org/10.1083/jcb.201705160>
- Devreotes, P.N., S. Bhattacharya, M. Edwards, P.A. Iglesias, T. Lampert, and Y. Miao. 2017. Excitable Signal Transduction Networks in Directed Cell Migration. *Annu. Rev. Cell Dev. Biol.* 33:103–125. <https://doi.org/10.1146/annurev-cellbio-100616-060739>
- Dormann, D., G. Weijer, S. Dowler, and C.J. Weijer. 2004. In vivo analysis of 3-phosphoinositide dynamics during Dictyostelium phagocytosis and chemotaxis. *J. Cell Sci.* 117:6497–6509. <https://doi.org/10.1242/jcs.01579>
- Dürrwang, U., S. Fujita-Becker, M. Erent, F.J. Kull, G. Tsiavaliaris, M.A. Geeves, and D.J. Manstein. 2006. Dictyostelium myosin-IE is a fast molecular motor involved in phagocytosis. *J. Cell Sci.* 119:550–558. <https://doi.org/10.1242/jcs.02774>
- Faix, J., L. Kreppel, G. Shaulsky, M. Schleicher, and A.R. Kimmel. 2004. A rapid and efficient method to generate multiple gene disruptions in Dictyostelium discoideum using a single selectable marker and the Cre-loxP system. *Nucleic Acids Res.* 32:e143. <https://doi.org/10.1093/nar/gnh136>
- Fort, L., J.M. Batista, P.A. Thomason, H.J. Spence, J.A. Whitelaw, L. Tweedy, J. Greaves, K.J. Martin, K.I. Anderson, P. Brown, et al. 2018. Fam49/CYRI interacts with Rac1 and locally suppresses protrusions. *Nat. Cell Biol.* 20:1159–1171. <https://doi.org/10.1038/s41556-018-0198-9>
- Funamoto, S., K. Milan, R. Meili, and R.A. Firtel. 2001. Role of phosphatidylinositol 3' kinase and a downstream pleckstrin homology domain-containing protein in controlling chemotaxis in dictyostelium. *J. Cell Biol.* 153:795–810. <https://doi.org/10.1083/jcb.153.4.795>
- Funamoto, S., R. Meili, S. Lee, L. Parry, and R.A. Firtel. 2002. Spatial and temporal regulation of 3-phosphoinositides by PI 3-kinase and PTEN mediates chemotaxis. *Cell.* 109:611–623. [https://doi.org/10.1016/S0092-8674\(02\)00755-9](https://doi.org/10.1016/S0092-8674(02)00755-9)
- Goehring, N.W., and S.W. Grill. 2013. Cell polarity: mechanochemical patterning. *Trends Cell Biol.* 23:72–80. <https://doi.org/10.1016/j.tcb.2012.10.009>
- Goulden, B.D., J. Pacheco, A. Dull, J.P. Zewe, A. Deiters, and G.R.V. Hammond. 2019. A high-avidity biosensor reveals plasma membrane PI(3,4)P₂ is predominantly a class I PI3K signaling product. *J. Cell Biol.* 218:1066–1079. <https://doi.org/10.1083/jcb.201809026>
- Graziano, B.R., and O.D. Weiner. 2014. Self-organization of protrusions and polarity during eukaryotic chemotaxis. *Curr. Opin. Cell Biol.* 30:60–67. <https://doi.org/10.1016/j.ccb.2014.06.007>
- Hacker, U., R. Albrecht, and M. Maniak. 1997. Fluid-phase uptake by macropinocytosis in Dictyostelium. *J. Cell Sci.* 110:105–112.
- Hoeller, O., and R.R. Kay. 2007. Chemotaxis in the absence of PIP3 gradients. *Curr. Biol.* 17:813–817. <https://doi.org/10.1016/j.cub.2007.04.004>
- Hoeller, O., P. Bolourani, J. Clark, L.R. Stephens, P.T. Hawkins, O.D. Weiner, G. Weeks, and R.R. Kay. 2013. Two distinct functions for PI3-kinases in macropinocytosis. *J. Cell Sci.* 126:4296–4307. <https://doi.org/10.1242/jcs.134015>
- Huang, Y.E., M. Iijima, C.A. Parent, S. Funamoto, R.A. Firtel, and P. Devreotes. 2003. Receptor-mediated regulation of PI3Ks confines PI(3,4,5)P₃ to the leading edge of chemotaxing cells. *Mol. Biol. Cell.* 14:1913–1922. <https://doi.org/10.1091/mbc.e02-10-0703>
- Ibarra, N., S.L. Blagg, F. Vazquez, and R.H. Insall. 2006. Nap1 regulates Dictyostelium cell motility and adhesion through SCAR-dependent and -independent pathways. *Curr. Biol.* 16:717–722. <https://doi.org/10.1016/j.cub.2006.02.068>
- Iijima, M., and P. Devreotes. 2002. Tumor suppressor PTEN mediates sensing of chemoattractant gradients. *Cell.* 109:599–610. [https://doi.org/10.1016/S0092-8674\(02\)00745-6](https://doi.org/10.1016/S0092-8674(02)00745-6)
- Insall, R.H., J. Borleis, and P.N. Devreotes. 1996. The aimless RasGEF is required for processing of chemotactic signals through G-protein-coupled receptors in Dictyostelium. *Curr. Biol.* 6:719–729. [https://doi.org/10.1016/S0960-9822\(09\)00453-9](https://doi.org/10.1016/S0960-9822(09)00453-9)
- Janetopoulos, C., and P. Devreotes. 2006. Phosphoinositide signaling plays a key role in cytokinesis. *J. Cell Biol.* 174:485–490. <https://doi.org/10.1083/jcb.200603156>
- Junemann, A., V. Filić, M. Winterhoff, B. Nordholz, C. Litschko, H. Schwel-lenbach, T. Stephan, I. Weber, and J. Faix. 2016. A Diaphanous-related formin links Ras signaling directly to actin assembly in macropinocytosis and phagocytosis. *Proc. Natl. Acad. Sci. USA.* 113:E7464–E7473. <https://doi.org/10.1073/pnas.1611024113>
- Jung, G., K. Remmert, X. Wu, J.M. Volosky, and J.A. Hammer III. 2001. The Dictyostelium CARMIL protein links capping protein and the Arp2/3 complex to type I myosins through their SH3 domains. *J. Cell Biol.* 153:1479–1497. <https://doi.org/10.1083/jcb.153.7.1479>
- Kamimura, Y., Y. Xiong, P.A. Iglesias, O. Hoeller, P. Bolourani, and P.N. Devreotes. 2008. PIP3-independent activation of TorC2 and PKB at the cell's leading edge mediates chemotaxis. *Curr. Biol.* 18:1034–1043. <https://doi.org/10.1016/j.cub.2008.06.068>
- King, J.S., and R.R. Kay. 2019. The origins and evolution of macropinocytosis. *Philos. Trans. R. Soc. Lond. B Biol. Sci.* 374:20180158. <https://doi.org/10.1098/rstb.2018.0158>
- King, J.S., D.M. Veltman, M. Georgiou, B. Baum, and R.H. Insall. 2010. SCAR/WAVE is activated at mitosis and drives myosin-independent cytokinesis. *J. Cell Sci.* 123:2246–2255. <https://doi.org/10.1242/jcs.063735>
- Klarlund, J.K., A. Guilherme, J.J. Holik, J.V. Virbasius, A. Chawla, and M.P. Czech. 1997. Signaling by phosphoinositide-3,4,5-trisphosphate through proteins containing pleckstrin and Sec7 homology domains. *Science.* 275:1927–1930. <https://doi.org/10.1126/science.275.5308.1927>
- Kobe, B., and A.V. Kajava. 2001. The leucine-rich repeat as a protein recognition motif. *Curr. Opin. Struct. Biol.* 11:725–732. [https://doi.org/10.1016/S0959-440X\(01\)00266-4](https://doi.org/10.1016/S0959-440X(01)00266-4)
- Lemmon, M.A. 2004. Pleckstrin homology domains: not just for phosphoinositides. *Biochem. Soc. Trans.* 32:707–711. <https://doi.org/10.1042/BST0320707>
- Litschko, C., J. Linkner, S. Brühmann, T.E.B. Stradal, T. Reinl, L. Jänsch, K. Rottner, and J. Faix. 2017. Differential functions of WAVE regulatory complex subunits in the regulation of actin-driven processes. *Eur. J. Cell Biol.* 96:715–727. <https://doi.org/10.1016/j.ejcb.2017.08.003>
- Litschko, C., S. Brühmann, A. Csizsár, T. Stephan, V. Dimchev, J. Damiano-Guercio, A. Junemann, S. Körber, M. Winterhoff, B. Nordholz, et al. 2019. Functional integrity of the contractile actin cortex is safeguarded by multiple Diaphanous-related formins. *Proc. Natl. Acad. Sci. USA.* 116:3594–3603. <https://doi.org/10.1073/pnas.1821638116>
- Loovers, H.M., A. Kortholt, H. de Groote, L. Whitty, R.L. Nussbaum, and P.J. van Haaster. 2007. Regulation of phagocytosis in Dictyostelium by the inositol 5-phosphatase OCRL homolog Dd5P4. *Traffic.* 8:618–628. <https://doi.org/10.1111/j.1600-0854.2007.00546.x>
- Machesky, L.M., R.D. Mullins, H.N. Higgs, D.A. Kaiser, L. Blanchoin, R.C. May, M.E. Hall, and T.D. Pollard. 1999. Scar, a WASP-related protein, activates nucleation of actin filaments by the Arp2/3 complex. *Proc. Natl. Acad. Sci. USA.* 96:3739–3744. <https://doi.org/10.1073/pnas.96.7.3739>
- Maekawa, M., S. Terasaka, Y. Mochizuki, K. Kawai, Y. Ikeda, N. Araki, E.Y. Skolnik, T. Taguchi, and H. Arai. 2014. Sequential breakdown of

- 3-phosphorylated phosphoinositides is essential for the completion of macropinocytosis. *Proc. Natl. Acad. Sci. USA*. 111:E978–E987. <https://doi.org/10.1073/pnas.1311029111>
- Martin-Belmonte, F., and M. Perez-Moreno. 2012. Epithelial cell polarity, stem cells and cancer. *Nat. Rev. Cancer*. 12:23–38. <https://doi.org/10.1038/nrc3169>
- Meili, R., C. Ellsworth, S. Lee, T.B. Reddy, H. Ma, and R.A. Firtel. 1999. Chemoattractant-mediated transient activation and membrane localization of Akt/PKB is required for efficient chemotaxis to cAMP in Dictyostelium. *EMBO J*. 18:2092–2105. <https://doi.org/10.1093/emboj/18.8.2092>
- Michael, M., and S. Vermeren. 2019. A neutrophil-centric view of chemotaxis. *Essays Biochem*. 63:607–618. <https://doi.org/10.1042/EBC20190011>
- Miki, H., S. Suetsugu, and T. Takenawa. 1998. WAVE, a novel WASP-family protein involved in actin reorganization induced by Rac. *EMBO J*. 17:6932–6941. <https://doi.org/10.1093/emboj/17.23.6932>
- Moore, S.L., J.H. Sabry, and J.A. Spudich. 1996. Myosin dynamics in live Dictyostelium cells. *Proc. Natl. Acad. Sci. USA*. 93:443–446. <https://doi.org/10.1073/pnas.93.1.443>
- Parent, C.A., B.J. Blacklock, W.M. Froehlich, D.B. Murphy, and P.N. Devreotes. 1998. G protein signaling events are activated at the leading edge of chemotactic cells. *Cell*. 95:81–91. [https://doi.org/10.1016/S0092-8674\(00\)81784-5](https://doi.org/10.1016/S0092-8674(00)81784-5)
- Park, W.S., W.D. Heo, J.H. Whalen, N.A. O'Rourke, H.M. Bryan, T. Meyer, and M.N. Teruel. 2008. Comprehensive identification of PIP₃-regulated PH domains from *C. elegans* to *H. sapiens* by model prediction and live imaging. *Mol. Cell*. 30:381–392. <https://doi.org/10.1016/j.molcel.2008.04.008>
- Ramalingam, N., C. Franke, E. Jaschinski, M. Winterhoff, Y. Lu, S. Brühmann, A. Junemann, H. Meier, A.A. Noegel, I. Weber, et al. 2015. A resilient formin-derived cortical actin meshwork in the rear drives actomyosin-based motility in 2D confinement. *Nat. Commun*. 6:8496. <https://doi.org/10.1038/ncomms9496>
- Remmert, K., T.E. Olszewski, M.B. Bowers, M. Dimitrova, A. Ginsburg, and J.A. Hammer III. 2004. CARMIL is a bona fide capping protein interactant. *J. Biol. Chem*. 279:3068–3077. <https://doi.org/10.1074/jbc.M308829200>
- Rodriguez-Boulan, E., and I.G. Macara. 2014. Organization and execution of the epithelial polarity programme. *Nat. Rev. Mol. Cell Biol*. 15:225–242. <https://doi.org/10.1038/nrm3775>
- Sasaki, A.T., C. Chun, K. Takeda, and R.A. Firtel. 2004. Localized Ras signaling at the leading edge regulates PI3K, cell polarity, and directional cell movement. *J. Cell Biol*. 167:505–518. <https://doi.org/10.1083/jcb.200406177>
- Schaks, M., S.P. Singh, F. Kage, P. Thomason, T. Klünemann, A. Steffen, W. Blankenfeldt, T.E. Stradal, R.H. Insall, and K. Rottner. 2018. Distinct Interaction Sites of Rac GTPase with WAVE Regulatory Complex Have Non-redundant Functions in Vivo. *Curr. Biol*. 28:3674–3684.e6. <https://doi.org/10.1016/j.cub.2018.10.002>
- Seastone, D.J., E. Harris, L.A. Temesvari, J.E. Bear, C.L. Saxe, and J. Cardelli. 2001. The WASp-like protein scar regulates macropinocytosis, phagocytosis and endosomal membrane flow in Dictyostelium. *J. Cell Sci*. 114:2673–2683.
- Servant, G., O.D. Weiner, E.R. Neptune, J.W. Sedat, and H.R. Bourne. 1999. Dynamics of a chemoattractant receptor in living neutrophils during chemotaxis. *Mol. Biol. Cell*. 10:1163–1178. <https://doi.org/10.1091/mbc.10.4.1163>
- Servant, G., O.D. Weiner, P. Herzmark, T. Balla, J.W. Sedat, and H.R. Bourne. 2000. Polarization of chemoattractant receptor signaling during neutrophil chemotaxis. *Science*. 287:1037–1040. <https://doi.org/10.1126/science.287.5455.1037>
- Sobczyk, G.J., J. Wang, and C.J. Weijer. 2014. SILAC-based proteomic quantification of chemoattractant-induced cytoskeleton dynamics on a second to minute timescale. *Nat. Commun*. 5:3319. <https://doi.org/10.1038/ncomms4319>
- Stark, B.C., M.H. Lanier, and J.A. Cooper. 2017. CARMIL family proteins as multidomain regulators of actin-based motility. *Mol. Biol. Cell*. 28:1713–1723. <https://doi.org/10.1091/mbc.e17-01-0019>
- Steffen, A., J. Faix, G.P. Resch, J. Linkner, J. Wehland, J.V. Small, K. Rottner, and T.E.B. Stradal. 2006. Filopodia formation in the absence of functional WAVE- and Arp2/3-complexes. *Mol. Biol. Cell*. 17:2581–2591. <https://doi.org/10.1091/mbc.e05-11-1088>
- Stuelten, C.H., C.A. Parent, and D.J. Montell. 2018. Cell motility in cancer invasion and metastasis: insights from simple model organisms. *Nat. Rev. Cancer*. 18:296–312. <https://doi.org/10.1038/nrc.2018.15>
- Swaney, K.F., C.H. Huang, and P.N. Devreotes. 2010. Eukaryotic chemotaxis: a network of signaling pathways controls motility, directional sensing, and polarity. *Annu. Rev. Biophys*. 39:265–289. <https://doi.org/10.1146/annurev.biophys.093008.131228>
- Swaney, K.F., J. Borleis, P.A. Iglesias, and P.N. Devreotes. 2015. Novel protein Callipygian defines the back of migrating cells. *Proc. Natl. Acad. Sci. USA*. 112:E3845–E3854. <https://doi.org/10.1073/pnas.1509098112>
- Tuxworth, R.I., I. Weber, D. Wessels, G.C. Addicks, D.R. Soll, G. Gerisch, and M.A. Titus. 2001. A role for myosin VII in dynamic cell adhesion. *Curr. Biol*. 11:318–329. [https://doi.org/10.1016/S0960-9822\(01\)00097-5](https://doi.org/10.1016/S0960-9822(01)00097-5)
- Tweedy, L., D.A. Knecht, G.M. Mackay, and R.H. Insall. 2016. Self-Generated Chemoattractant Gradients: Attractant Depletion Extends the Range and Robustness of Chemotaxis. *PLoS Biol*. 14:e1002404. <https://doi.org/10.1371/journal.pbio.1002404>
- Veltman, D.M., G. Akar, L. Bosgraaf, and P.J. Van Haastert. 2009. A new set of small, extrachromosomal expression vectors for Dictyostelium discoideum. *Plasmid*. 61:110–118. <https://doi.org/10.1016/j.plasmid.2008.11.003>
- Veltman, D.M., M.G. Lemieux, D.A. Knecht, and R.H. Insall. 2014. PIP₃-dependent macropinocytosis is incompatible with chemotaxis. *J. Cell Biol*. 204:497–505. <https://doi.org/10.1083/jcb.201309081>
- Veltman, D.M., T.D. Williams, G. Bloomfield, B.C. Chen, E. Betzig, R.H. Insall, and R.R. Kay. 2016. A plasma membrane template for macropinocytotic cups. *eLife*. 5:e20085. <https://doi.org/10.7554/eLife.20085>
- Woznica, D., and D.A. Knecht. 2006. Under-agarose chemotaxis of Dictyostelium discoideum. *Methods Mol. Biol*. 346:311–325.
- Xiao, Z., N. Zhang, D.B. Murphy, and P.N. Devreotes. 1997. Dynamic distribution of chemoattractant receptors in living cells during chemotaxis and persistent stimulation. *J. Cell Biol*. 139:365–374. <https://doi.org/10.1083/jcb.139.2.365>
- Zwolak, A., C. Yang, E.A. Feeser, E.M. Ostap, T. Svitkina, and R. Dominguez. 2013. CARMIL leading edge localization depends on a non-canonical PH domain and dimerization. *Nat. Commun*. 4:2523. <https://doi.org/10.1038/ncomms3523>

Supplemental material

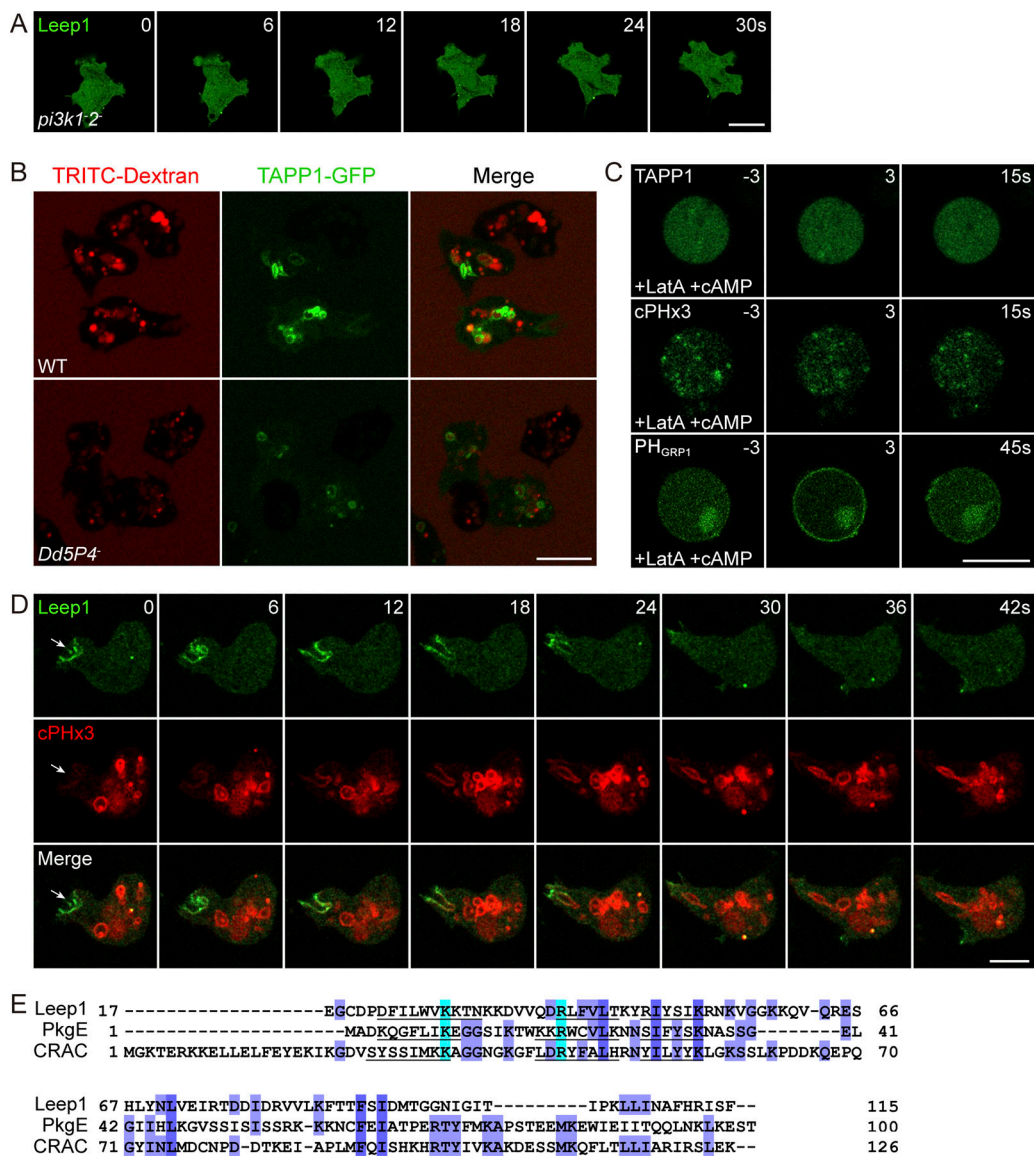


Figure S1. **Regulation of the membrane association of Leep1.** (A) Time-lapse imaging of GFP-Leep1/*pi3k1*⁻² cells during under-agarose chemotaxis. (B) *Dd5P4*⁻ cells exhibited reduced TAPP1-GFP signal and dextran uptake. (C) Translocation of GFP-tagged TAPP1, cPHx3, and PH_{GRP1} in response to cAMP stimulation in the presence of LatA. (D) Sequential accumulation of GFP-Leep1 and RFP-cPHx3. GFP-Leep1 was selectively enriched at membrane ruffles and macropinosomes and quickly removed from internalized macropinosomes, whereas the signal of cPHx3 gradually increased until a peak was reached after the macropinosomes detached from the cell surface. (E) Sequence alignment of Leep1 with PH domains from CRAC or PkgE revealed a PH-like fold within the N terminus of Leep1. Cyan shading indicates the two positively charged residues (K28 and R39) mutated in Leep1^{AA}. Scale bar = 10 μm.

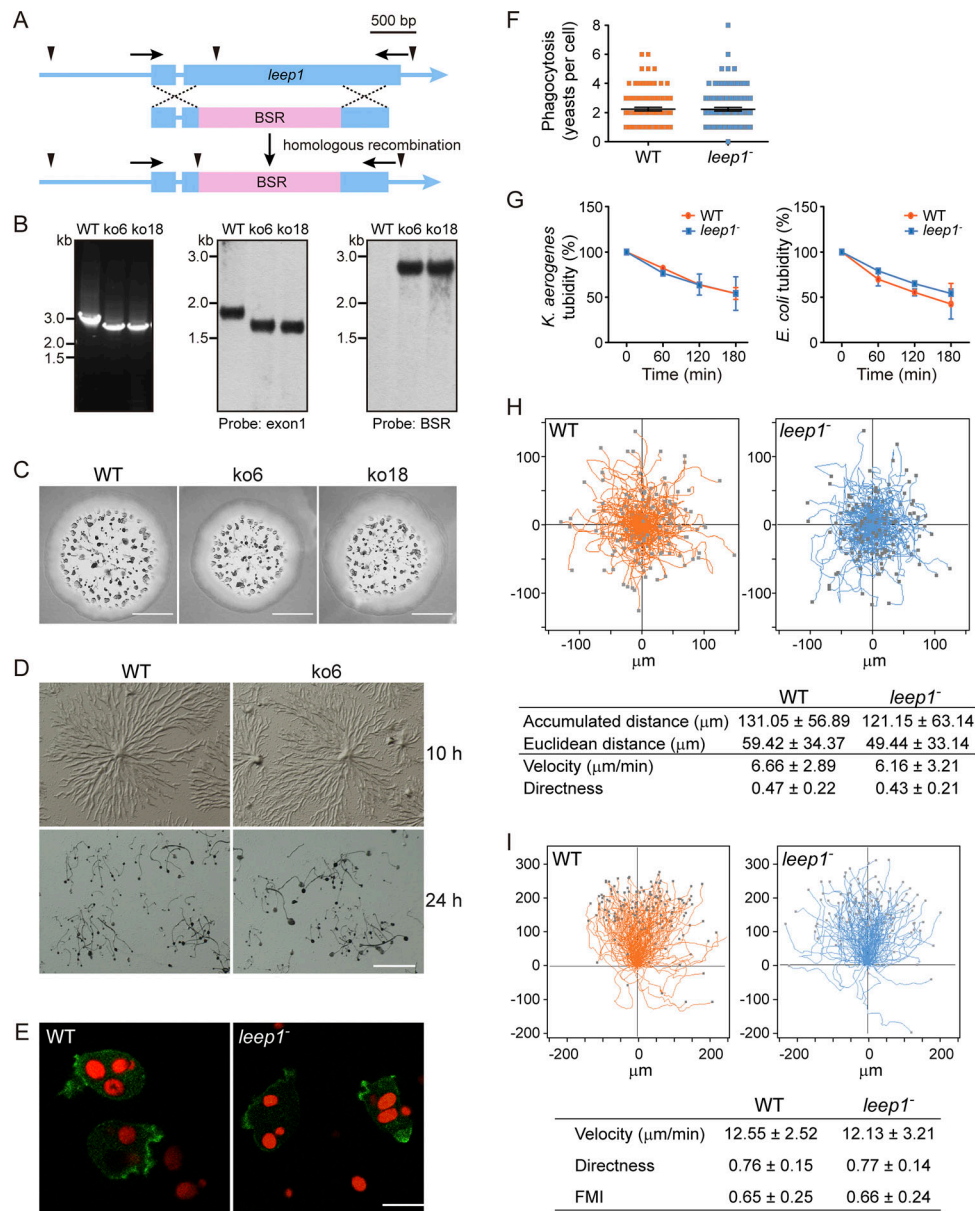


Figure S2. **Generation and characterization of *leep1* knockout (ko) cells.** (A) Design of the knockout construct. A blasticidin resistant cassette (BSR) was inserted to replace part of the open reading frame of *leep1*. Arrowheads mark the sites where genomic DNA was digested. (B) Targeted clones were confirmed by PCR and Southern blotting. (C) WT and *leep1⁻* cells were plated clonally with bacteria (*Klebsiella aerogenes*) on standard medium agar for 5 d. Scale bar = 5 mm. (D) WT and *leep1⁻* cells were plated as a monolayer on non-nutrient agar to induce development. Typical fields of view were photographed at the indicated time points. Scale bar = 2 mm. (E) Accumulation of TRITC-labeled yeast particles by phagocytosis. Scale bar = 5 μm . (F) Quantification of yeast phagocytosis. (G) Phagocytosis of *K. aerogenes* or *Escherichia coli* measured by the decreasing turbidity after addition of WT or *leep1⁻* cells. Data were from three independent experiments and represent mean \pm SD. (H) Top: Trajectories of randomly migrating cells ($n = 142$ for WT and 168 for *leep1⁻*). Bottom: Summary of the respective motility parameters (mean \pm SD). (I) Top: Trajectories of cells migrating under agarose against a passive gradient of folate ($n = 155$ for WT and 129 for *leep1⁻*). Bottom: Summary of the respective chemotaxis parameters (mean \pm SD). Data are from three independent experiments. FMI, forward migration index.

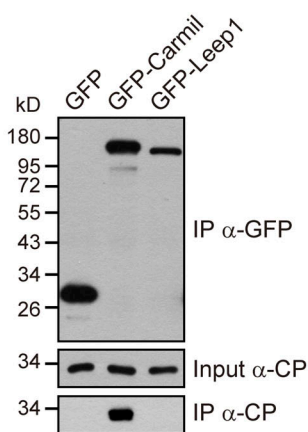
A

Leep1	1	MSEELSTGTEKRFVFDLEGCDPDFLWKK-----TNKKDVVQDLFVLTQYRISYIKRNKVGKKQVQRESHLYNLVEIRTDID	80
dCarmil	1	MSEELSPNDRKFIINLLTQKNQESLLSIGDKISKKNKKPSKRILILITKNRIFFLKPSQ----NKVKKDIHLLDIQEIKSSTSN	81
Leep1	81	RVVLKF----TTFSIDMTGGNIGITIPKLLINAFHRISFTFSNEALPNLLILPPERITAPEVDEIDPGQSHGFFVYRAQCNYYDT	161
dCarmil	82	EFTIVAKVDNKQFSYGLINTKTDEIINQIR-VTINHQFGCPESTFKCTDIKDSR-LVEI-EQKDLPCGGFVETYSIQCDHLGV	163
Leep1	162	PVNQDLIDYLEE-TVSKGSRVFNLDFFAGIDRNSEGAVNLTPVLAALRHNTFFDTFVCHNKTRKE-IPLLLADVFHHNRITLVRVD	244
dCarmil	164	PPRDDICWDMTNIISSKNIRSFNIGEL---ELPTSAGDTIRCLLGALKYNNYFKSFFNFNNYTFNKEQFGYLAELVKCNSTVEDLS	245
Leep1	245	LSGIESD-DGWQLGDALKENQTNQLVSLNCSNDRVSDKGMNSLANAIRSFNRPFLFIFASNVDLQSKGASIFFRITLQSNYSSSG	328
dCarmil	246	LNNVGLKHDTMPIATALLSSNKNLALTAIDISNNQIEDKGMTAFSSYVASLSLRGIASLDVSNNTCNKAGISVLTNALKKNIKMS	330
Leep1	329	AIVHLDVSRNDLEKIGSESLHDWIILLNTSIPSPRKPLVHINLEETQLDTTKVTMALKQGQLESLEYINLSGNKFTPEAVANLCS	413
dCarmil	331	TLSYLNLSGNKMEADGSAGLSSFLASPNTL-----KTLNISNTTPSMETIVGALVI-GCAELKTIIDISDNKLTKEKVPPLVR	406
Leep1	414	ITAKCDLSAQIKLSKCSITGDQVNNILNACTSGIQVHRTLDLSSNLEQKGLSFAQT-IKSSSNIAHLLNANNSFRKKGITFI	497
dCarmil	407	FIGASSTLKHFNLSGTVKVPVENLKELVVAITSNLYLQDVVLDLKNNDLGIAGARMLASLATDKLSNVIYLDVSENDGDEGVSVI	491
Leep1	498	VQALEENSTLQSIDLSSNFKSSSKAEP---VDHARTVHHHVSIRKLVLAGSVSKGFYLGKELLPVKSIVNDCKLEVELDISGNN	580
dCarmil	492	CDGFVGNSTIKKLLINGNEFKSKTKSRPSAIESVISLLESECEPLETHMTVG-NSKSPKADILSLIYSLATNSGLELDISGHQ	575
Leep1	581	MGDDICREIFESLKKNTCLKTLHLNNSLGLAGFOAMKRTFTTNRLLIDIPVPTADITKILNSNSKDKKQINDKIGEILADVQTC	665
dCarmil	576	MGPKGAIGLKGALQTNKTLHTLIWDDNLTTAIGFAGFQVGLERNLTLKNMPTPLNDIIQCHRE-----PKFQQIWKEDISC	651
Leep1	666	LSNNKNGIAYTDIPSTTKTTVAISSISTPNFRASITYHNSSS-----NNLGN-----DD---TYNRAASTHNLSYSSPS	731
dCarmil	652	INRQSPTRAFEGNG--GNSIGATN---LSFLASGQQQGVKLLNKIKSIRGRKVTDPNNILIVKDAESTEKVIGGIIHLIKESIHA	731
Leep1	732	PSTY*APPPPL-----PDVYANHYQQPPPPPPQEYDYSQQHQYDYDYSQQQQQQQQYDYSQQHTDQQQ	794
dCarmil	732	SLEMELNQLKDFVQVNDVINAKKNEMTQQILESMQNTFQSMGPTIKR-----LATTIQYGSKDQVDEQQ	797
Leep1	795	YDYQ-----AQDYQEGATTNDYDQQYQQQDYDQQYDQQQQQYDQQQHYDQQQYEDENRMPPP--FEY----	861
dCarmil	798	IHSTLVKGGAGAEISSRAHECFISALDIASDYTYEKITIGLDSVFKDLILEESQAQNEASGATPIPDSVPVTRSPQTSPIITQP	882
Leep1	883	TPTTNVPPVTAPRTGAAAPLKPANPPVSTTTTPPVSTTPKPTQPVSKFGAKLSANSVAEAIARNMGGGAPPIRKPVAPEPEPE	967
Leep1	968	PVPTTKDVTPLKSKPVVAPRSPTTSTPTKTPVKKPSGSPVPGSLSDAPESDSAEI THVTASRPH IASKRKPPTRRPRPPTEN	1050

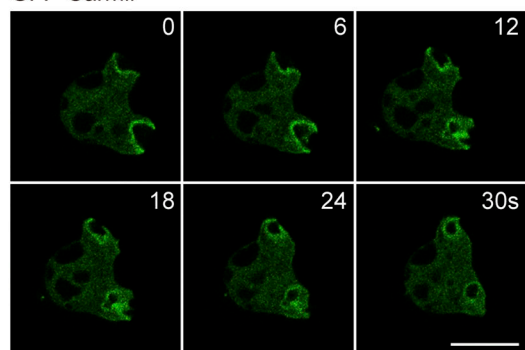
B

	-----LxHxTxRPKxxxxxP-----
<i>Dictyostelium</i>	-DAPESDSAEI THVTASRPH IASKRKPPTRRPRPP-
<i>Acanthamoeba</i>	TELEAA-ESNLTHMTKDRPMGPRRRRQQRKQRRP-
<i>C.elegans</i>	-DLPPK-PSVLSHLQKARPKRGGASSILNSSLSE-
<i>Drosophila</i>	-ELPSA-SFQLQHLVKGGRPKRAKTRAPTRP----
hCARMIL1	--LPSEEGKLEHFTKLRPKRNKKQQPTQAAVCAA-
hCARMIL2	-DLPLA-GQPLRHPTRARPRRR-QHHHRPPGGPQ
hCARMIL3	-ELPTH-GYKLRHQIQGRPRPPR-TTP--PGGRPS

C



D GFP-Carmil



E

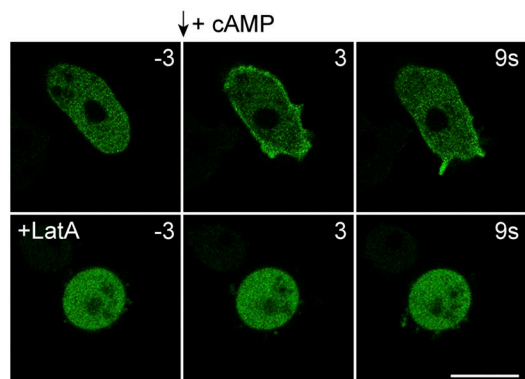


Figure S3. **Dictyostelium Carmil, but not Leep1, interacts with CPs.** (A) Sequence alignment of Leep1 and *Dictyostelium* Carmil. Orange box, pink box, cyan box, and green underline indicate the verprolin-like region, acidic region, CP interaction motif, and proline-rich domain in Carmil, respectively. The red asterisk marks A736 in Leep1. (B) Sequence alignment of CP interactions from selected CARMILs. Cyan shading indicates residues that are identical to the consensus sequence shown at the top. (C) Immunoprecipitation performed using GFP-trap agarose. Samples were immunoblotted with anti-GFP or anti-CP antibody. (D) Time-lapse imaging of GFP-Carmil in vegetative cells. (E) Time-lapse imaging of GFP-Carmil in cells responding to cAMP stimulation in the absence or presence of LatA. Scale bar = 10 μ m. *C. elegans*, *Caenorhabditis elegans*; IP, immunoprecipitation.

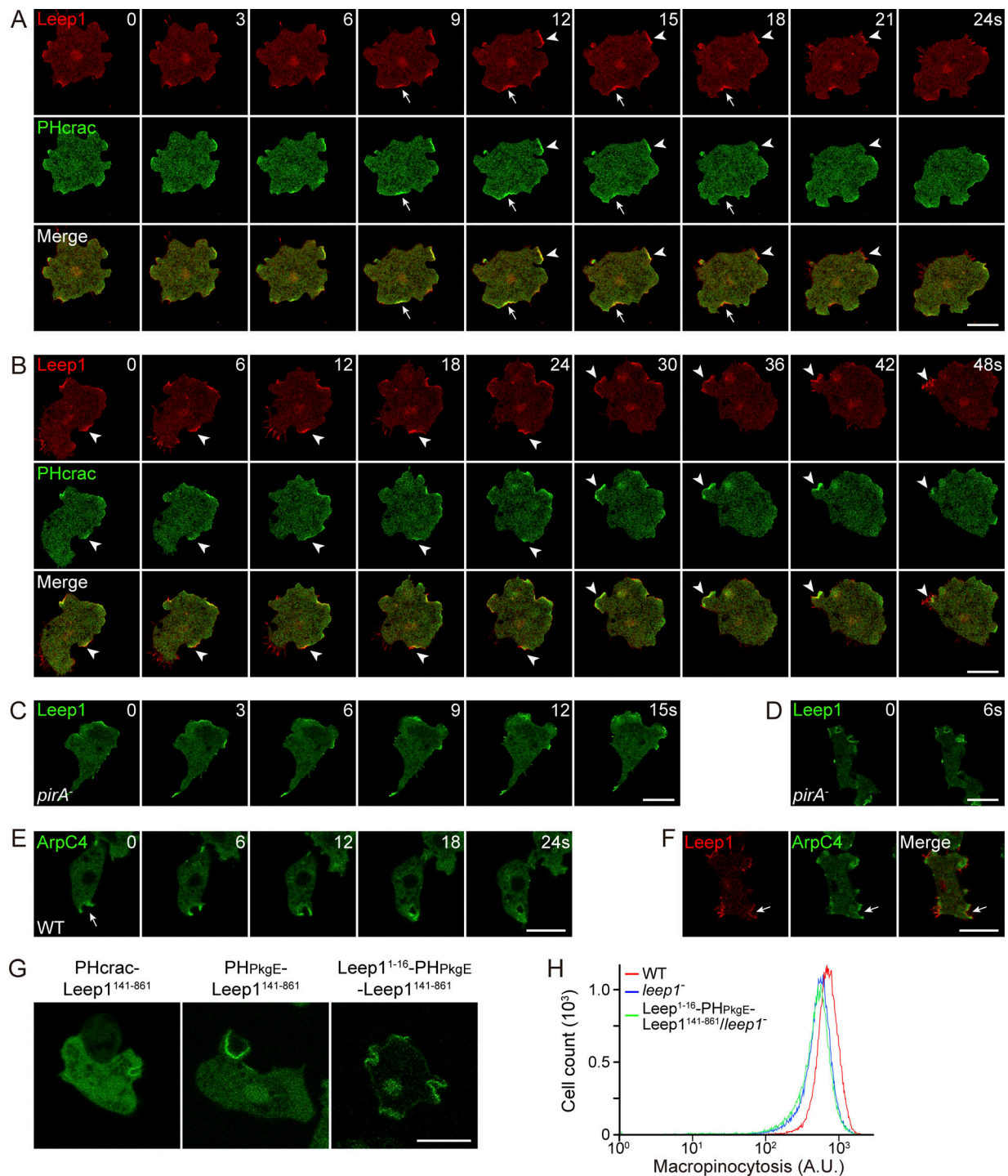


Figure S4. **Regulation of the localization and function of Leep1.** (A and B) Time-lapse imaging of WT cells expressing RFP-Leep1 and PHcrac-GFP during under-agarose chemotaxis. RFP-Leep1 largely colocalized with PHcrac-GFP at pseudopods and during their retraction (indicated by the arrowheads) or splitting (indicated by the arrows). (C and D) Time-lapse imaging of GFP-Leep1/*pirA*⁻ cells during under-agarose chemotaxis (C) or macropinocytosis (D). PirA was not necessary for recruiting Leep1 to pseudopods or macropinocytic cups. (E) GFP-ArpC4 localization during macropinocytosis. (F) Localization of RFP-Leep1 and GFP-ArpC4 at macropinocytic cups. (G) Localization of GFP-tagged chimeric proteins, which were generated by replacing the N terminus of Leep1 with PHcrac or PHpkGE. (H) Flow cytometry analysis of cells incubated with TRITC-dextran for 30 min. Scale bar = 10 μm. A.U., arbitrary units.

Video 1. **Localization of GFP-Leep1 in response to cAMP stimulation and during macropinocytosis.** cAMP stimulation: cAMP-induced GFP-Leep1 translocation in differentiated WT cells. Corresponds to Fig. 2 A. Scale bar = 10 μm . Macropinocytosis: Localization of GFP-Leep1 in vegetative WT cells. Corresponds to Fig. 2 D. Images were captured at 6-s intervals and played back at 2 frames per second. Scale bar = 10 μm .

Video 2. **Localization of GFP-Leep1 in differentiated WT cells chemotaxing toward cAMP released by a micropipette placed at the right bottom corner.** Corresponds to Fig. 2 H. Images were captured at 10-s intervals and played back at 4 frames per second. Scale bar = 10 μm .

Video 3. **Localization of GFP-Leep1 in vegetative WT cells moving along a self-generated folate gradient under agarose.** Corresponds to Fig. 2 I. Images were captured at 2-s intervals and played back at 30 frames per second. Scale bar = 10 μm .

Video 4. **Localization of GFP-Leep1 and RFP-LimeAcoil in vegetative WT cells.** Corresponds to Fig. 2 J. Images were captured at 6-s intervals and played back at 5 frames per second. Scale bar = 10 μm .

Video 5. **PHcrac-GFP dynamics in vegetative WT and *leep1*⁻ cells.** Corresponds to Figure 4 E. Images were captured at 3-s intervals and played back at 25 frames per second. Scale bar = 10 μm .

Video 6. **WT and *leep1*⁻ cells moving along a self-generated folate gradient under agarose.** Corresponds to Fig. 4 I. Images were captured at 20-s intervals and played back at 15 frames per second. Scale bar = 50 μm .

Video 7. **WT or *leep1*⁻ cells expressing GFP-ArpC4 moving along folate gradients under agarose.** Graph showing tracks of GFP fluorescence intensities is inserted at the beginning of each video, with each pixel in the overlaid image corresponding the maximum pixel intensity for that location over the course of the video. Corresponds to Fig. 4 J. Images were captured at 2-s intervals and played back at 25 frames per second. Scale bar = 20 μm .

Video 8. **Localization of GFP-tagged full-length and truncated Leep1 overexpressed in vegetative WT cells.** Substrate-attached filopodia were detected by imaging in a lower focal plane. Images were captured at 6-s intervals and played back at 10 frames per second. Scale bar = 10 μm .

Video 9. **PirA-GFP^{REMI}/*pirA*⁻ and PirA-GFP^{REMI}/*pirA*⁻*leep1*⁻ cells migrating along folate gradients under agarose.** Corresponds to Fig. 6 I. Images were captured at 2-s intervals and played back at 6 frames per second. Scale bar = 10 μm .

Video 10. **PirA-GFP^{REMI}/*pirA*⁻ cells expressing RFP-Leep1 migrating along folate gradients under agarose.** Corresponds to Fig. 6, K and L. Images were captured at 2-s intervals and played back at 2 frames per second. Scale bar = 10 μm .

Four tables are provided online as separate Excel files. Table S1 shows proteins identified in MS analysis. Table S2 shows proteins with translocation scores ≥ 0.55 and temporal changes like PHcrac (score 10 s/score 0 s or score 20 s/score 0 s ≥ 1.3 and score 10 s/score 60 s or score 20 s/score 60 s ≥ 1.3). Table S3 shows proteins known or proposed to regulate leading (pink shade) or trailing edge (cyan shade) activities identified in the proteomics-based approach. Table S4 shows proteomic identification of Leep1-binding proteins.